

pubs.acs.org/JACS Perspective

Emerging Two-Dimensional Organic Semiconductor-Incorporated Perovskites—A Fascinating Family of Hybrid Electronic Materials

Jiaonan Sun, Kang Wang, Ke Ma, Jee Yung Park, Zih-Yu Lin, Brett M. Savoie, and Letian Dou*



Cite This: J. Am. Chem. Soc. 2023, 145, 20694-20715



Read Online

ACCESS I

III Metrics & More

Article Recommendations

ABSTRACT: Halide perovskites have attracted a great amount of attention owing to their unique materials chemistry, excellent electronic properties, and low-cost manufacturing. Two-dimensional (2D) halide perovskites, originating from three-dimensional (3D) perovskite structures, are structurally more diverse and therefore create functional possibilities beyond 3D perovskites. The much less restrictive size constraints on the organic component of these hybrid materials particularly provide an exciting platform for designing unprecedented materials and functionalities at the molecular level. In this Perspective, we discuss the concept and recent development of a sub-class of 2D perovskites, namely, organic semiconductor-incorporated perovskites (OSiPs). OSiPs combine the electronic functionality of organic semiconductors with the soft and dynamic halide perovskite lattice, offering opportunities for tailoring the energy landscape, lattice and carrier dynamics, and electron/ion transport properties for various fundamental studies, as well as device applications. Specifically, we summarize recent advances in the design, synthesis, and structural analysis of OSiPs with various organic conjugated moieties as well as the application of OSiPs in photovoltaics, light-emitting devices, and transistors. Lastly, challenges and further opportunities for OSiPs in molecular design, integration of novel functionality, film quality, and stability issues are addressed.

1. INTRODUCTION

The discovery of perovskite materials can be traced back to the 1800s, 1,2 but it was only in the past few decades that the halide perovskite family, first as transistor materials³ and then as light absorbers, attracted significant research interest. These materials are now recognized as prominent semiconductors for next-generation photovoltaics.^{51–8} The structure of halide perovskite is generalized to ABX₃, where A are monovalent cations, such as methylammonium (MA), formamidinium (FA), Cs, etc.; B are divalent metal cations; and X are halide anions (Figure 1a). Driven by the excellent optical absorption with a tunable band gap, high charge mobility, long carrier diffusion length, and low-cost processing, the state-of-the-art power conversion efficiency (PCE) of perovskite solar cells (PSCs) is approaching that of single-crystalline Si.⁶ However, environmental stability issues (i.e., degradation susceptibilities to heat, light, bias, and moisture) hinder the further development of perovskites. Reducing the dimensionality of perovskites in which the inorganic [BX₆]⁴⁻ sheets, chains, or even individual octahedra are isolated by organic molecules could be an effective approach to enhance the environmental stability. Among various low-dimensional perovskites, twodimensional (2D) perovskites, which maintain many key features of three-dimensional (3D) perovskites, have been extensively studied because of their tunable optoelectronic properties, rich chemical diversity, easy integration as heterostructures, and superior stability.

Most 2D perovskites with layered structures can be achieved through intercalating organic cations into the (100) plane of the parent 3D cubic structure, with n representing the number of $[BX_6]^{4-}$ inorganic layers that were capped by organic

ligands. Note that recently researchers have also reported the utilization of large inorganic spacer cations to form allinorganic 2D perovskites as a new subclass of perovskite materials, 9-11 yet the current discussion primarily focuses on hybrid organic-inorganic structures. Increasing the number of layers of inorganic sheets to infinity leads to the 3D perovskite structure illustrated in Figure 1a. The 2D perovskite (100) family includes three typical phases: Ruddlesden-Popper (RP), Dion-Jacobson (DJ), and alternating cations (ACI) (Figure 1b). 12,13 The RP-phase perovskite employs monovalent cationic organic ligands that form ionic bonding with the inorganic slab. Two organic layers are accommodated between two $[BX_6]^{4-}$ inorganic sheets with (1/2, 1/2)displacement. The general formula is $L_2A_{n-1}B_nX_{3n+1}$ ("L" represents a "ligand" or, more strictly speaking, a "bulky cation"). Note that the definition of "ligand" here is slightly different from that used in inorganic, colloidal, and biological chemistries. Here, to differentiate from the A- and B-site cations in perovskites, we name the bulky cation as a "ligand", not necessarily following any previous definitions of "ligand" in other areas of chemistry. The DJ-phase perovskite employs divalent organic ligands that interact with the inorganic slab from both sides, and therefore only one organic layer exists

Published: September 14, 2023





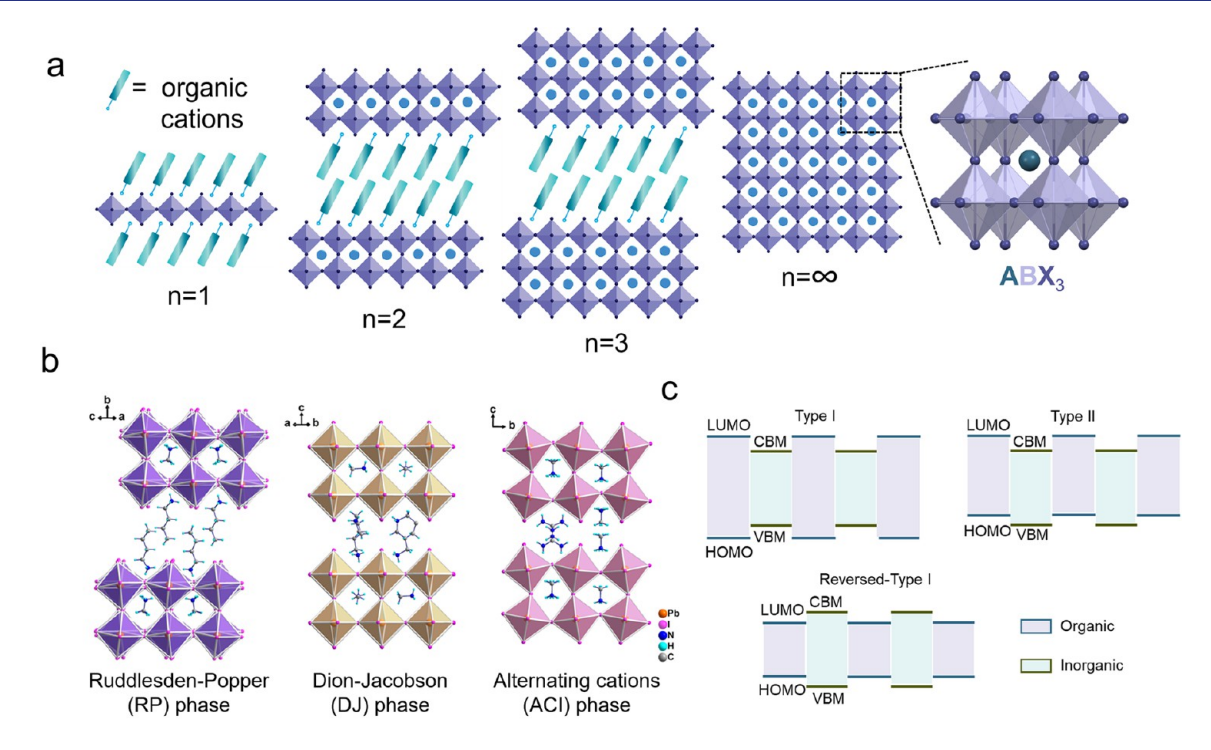


Figure 1. (a) Schematics of 2D (n = 1-3) and 3D perovskites. (b) RP, DJ, and ACI phases of 2D perovskite (from left to right). Reproduced with permission from ref 12. Copyright 2021 American Chemical Society. (c) Scheme of perovskite 2D quantum wells with type I, type II, and reversed-type I energy alignment.

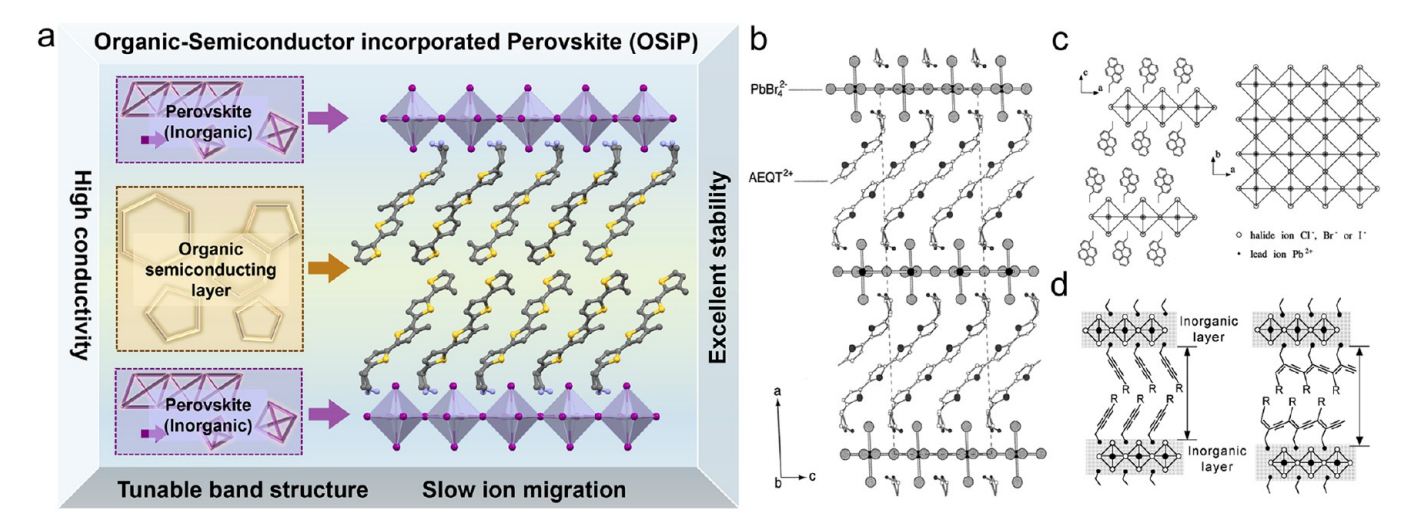


Figure 2. (a) Schematics of OSiPs and their advantages. Early-stage OSiPs with (b) AEQT (Reproduced with permission from ref 18. Copyright 1999 American Chemical Society.), (c) pyrene (Reproduced with permission from ref 19. Copyright 1999 Elsevier Science B.V.), and (d) polydiacetylene ligands (Reproduced with permission from ref 20. Copyright 2001 Royal Society of Chemistry.).

between $[BX_6]^{4-}$ inorganic sheets, without lattice displacement between the top and bottom layers. The general formula is $LA_{n-1}B_nX_{3n+1}$. An ACI phase with alternating order that uses guanidinium ligands and MA was demonstrated in Kanatzidis's work. Generally, 2D perovskites adopt a quantum-well structure with organic barriers and inorganic wells, in which the HOMO of organic ligands is deeper than the inorganic valence band maximum (VBM) and the LUMO is shallower than the inorganic conduction band minimum (CBM), as shown in Figure 1c, type I. The relatively large HOMO–LUMO gap comes from the insulating nature of the nonconjugated short-chain organic ligands. By incorporating

organic ligands with extended conjugation, the 2D quantum-well structure can be tuned from type I to type II or reversed-type I band alignment in the organic—inorganic hybrid structure (Figure 1c). To differentiate it from the conventional hybrid perovskites, this type of semiconducting 2D perovskite material, with the incorporation of functional conjugated organic cations, can be considered an "organic semiconductor-incorporated perovskite", abbreviated to "OSiP" (Figure 2a).

Although it had not been defined at that time, the history of OSiP can be traced back to more than 20 years ago. In 1999, Mitzi et al. designed the first functional divalent quater-

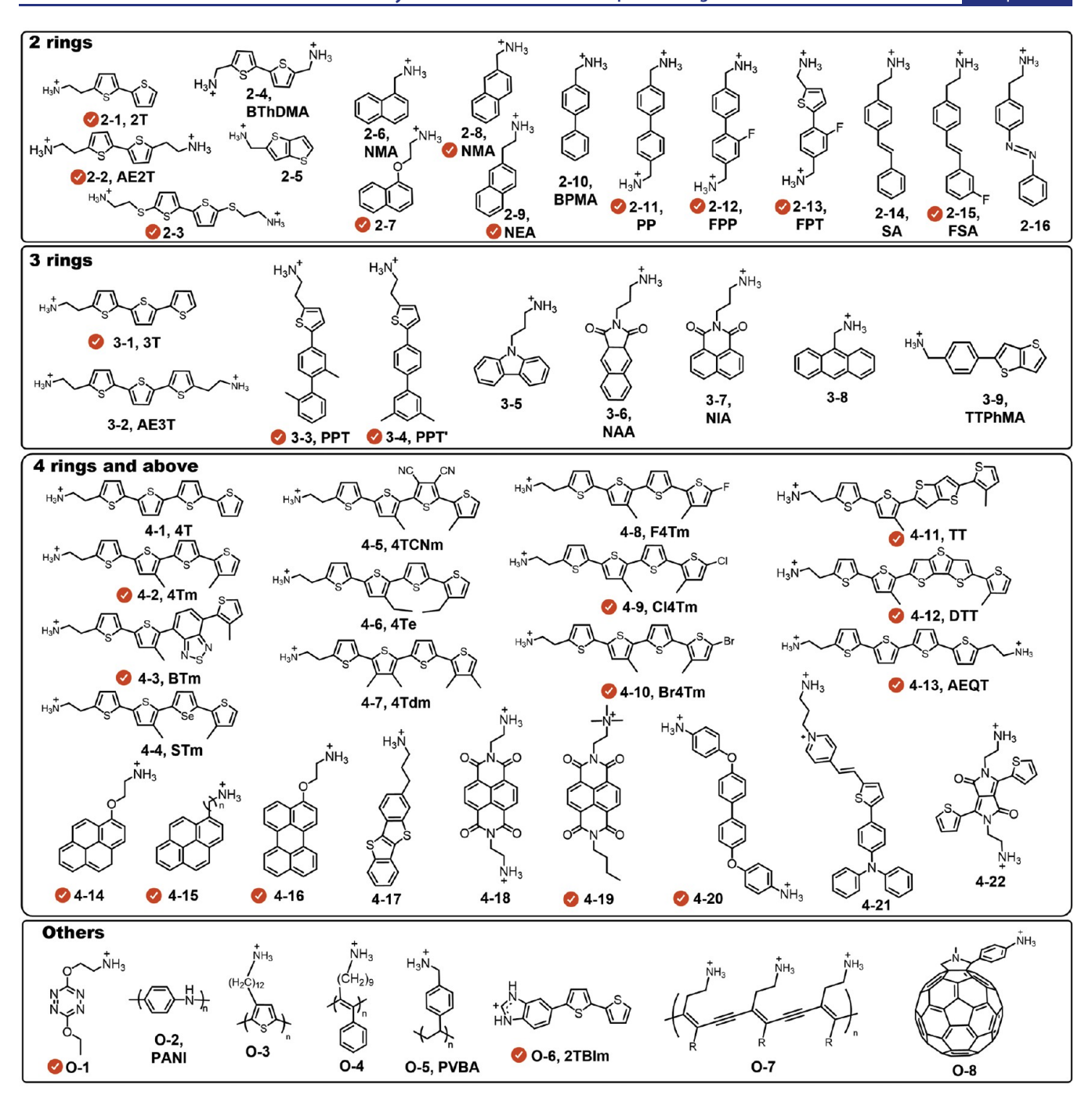


Figure 3. continued

ethan-1-aminium $(4\text{Te});^{59}$ 4-7, 2-(3',3''',4',4'''-tetramethyl-[2,2':5',2'':5'',2-quaterthiophen]-5-yl)ethan-1-aminium $(4\text{Tdm});^{59}$ 4-8, 2-(5'''-fluoro-3''',4'-dimethyl-[2,2':5',2'':5'',2''':5'',2''':5'',2-quaterthiophen]-5-yl)ethan-1-aminium $(F4\text{Tm});^{60}$ 4-9, 2-(5'''-chloro-3''',4'-dimethyl-[2,2':5',2'':5'',2''':5'',2''':5'',2-quaterthiophen]-5-yl)ethan-1-aminium $(F4\text{Tm});^{60}$ 4-9, 2-(5'''-chloro-3''',4'-dimethyl-[2,2':5',2'':5'',2''':5'',2''':5'',2'':5''phen]-5-yl)ethan-1-aminium (Cl4Tm); 60 4-10, 2-(5"-bromo-3",4'-dimethyl-[2,2':5',2":5",2"'-quaterthiophen]-5-yl)ethan-1-aminium (Br4Tm); 60 4-11, 2-(4'-methyl-5'-(5-(3-methylthiophen-2-yl)thiophen-2-yl)-[2,2'-bithiophen]-5-yl)ethan-1-aminium (TT); 4-12, 2-(4'-methyl-5'-(5-(3-methylthiophen-2-yl))-[2,2'-bithiophen]-5-yl)yl-5'-(6-(3-methylthiophen-2-yl)dithieno[3,2-b:2',3'-d]thiophen-2-yl)-[2,2'-bithiophen]-5-yl)ethan-1-aminium (DTT); 40 4-13, 2,2'-yl)propan-1-aminium; 4-18, 2,2'-(1,3,6,8-tetraoxo-1,3,6,8-tetrahydrobenzo[lmn][3,8]phenanthroline-2,7-diyl)bis(ethan-1-aminium); 4-19, 2-(7-butyl-1,3,6,8-tetraoxo-3,6,7,8-tetrahydrobenzo[lmn][3,8]phenanthrolin-2(1H)-yl)-N,N,N-trimethylethan-1-aminium; 64 4-20, 4,4'-([1,1'-biphen-1]) yl]-4,4'-diylbis(oxy))dibenzenaminium;²³ 4-21, (E)-1-(3-ammoniopropyl)-4-(2-(5-(4-(diphenylamino)phenyl)thiophen-2-yl)vinyl)pyridin-1ium; 65 4-22, 2 , 2 - $^$ 1-ammonium); 70 O-5, poly(vinylbenzylammonium) (PVBA); 71 O-6, 6-([2,2'-bithiophen]-5-yl)-1*H*-benzo[*d*]imidazol-3-ium (2TBIm); 30 O-7, polydiacetylene; 20,72 O-8, *N*-methyl-2-(4-aminophenyl)fulleropyrrolidine. 73

thiophene molecule (AEQT) and incorporated it into an inorganic perovskite framework to form DJ-phase 2D perovskites with a herringbone arrangement (Figure 2b). 18 The excitonic absorption feature and photoluminescence properties of perovskites changed with the different halides. In the same year, pyrene molecules were incorporated into the [PbX₆]⁴⁻ mixed-halide inorganic framework as chromophores by Braun et al. (Figure 2c).¹⁹ The increase in phosphorescence intensity and decrease in triplet-state lifetime from Cl to I were explained by the heavy-atom effect. Shortly after, in 2001, Takeoka and co-workers realized the polymerization within the [PbBr₆]⁴⁻ framework and formed OSiPs incorporating a polydiacetylene backbone (Figure 2d).²⁰ The solid-state polymerization reaction under γ -ray was confirmed by the occurrence of a new $\pi - \pi^*$ transition from UV-vis spectra. Despite OSiPs having a history of over 20 years, few dedicated efforts were made in this field before the burst of perovskite photovoltaics. ^{19–26} With a deep understanding of organic semiconducting materials and the importance of functional organic cations in hybrid 2D perovskite structures, in 2019 our group designed and synthesized a series of new thiophenebased monovalent ligands that form single-crystalline RP-phase OSiPs, establishing OSiPs as a new sub-class of hybrid halide perovskite materials featuring organic semiconducting ligands.^{27–29} Moreover, our group further extended the scope by designing more functional conjugated ligands, which were successfully incorporated into the 2D halide perovskite framework and were demonstrated to have excellent performance in a variety of electronic and optoelectronic devices.^{30–42}

The successful application of OSiPs in devices is closely related to several advantages: (1) With careful molecular design, a complete set of type I, type II, and reversed-type I energy alignment in perovskite quantum wells with intriguing optoelectronic properties can be achieved. (2) Through the approach of structural fine-tuning, it is possible to adjust the assembly of the organic barrier in 2D perovskite via secondary bonding interactions, thus improving the corresponding lattice tension and conductivity, which may benefit charge transport. (3) OSiP also offers a new playground for characterizing and understanding the photophysics of these self-organized heterostructures with new charge-transfer and energy-transfer features. (4) The organic conjugated molecules with rigid and hydrophobic nature within OSiPs serve as moisture and ion migration barriers, resulting in greatly enhanced stability compared to conventional short-chain 2D and 3D perovskite counterparts.

In this Perspective, we mainly discuss the structure and functionality of conjugated organic ligands, the structureproperty relationships of 2D OSiPs, and applications of OSiPs in solar cells, light-emitting diodes (LEDs), and field-effect transistors (FETs). In the end, the future direction of OSiP will be discussed, focusing on ligand design, novel functionality incorporation, film quality, and stability.

2. STRUCTURE AND PROPERTIES OF OSIPS

2.1. Molecular Design of Conjugated Ligands. Conjugated organic ligands contribute to the new electronic features in OSiPs. However, designing/synthesizing functional organic ligands with ideal geometry and realizing the successful incorporation of bulky conjugated ligands to form 2D perovskites require many empirical trials, and this remains challenging. One design criterion is to make full use of the outof-plane relaxation of 2D perovskites by increasing the conjugation of ligands to decrease the HOMO-LUMO gaps. At the same time, new ligands should maintain a small cross section to fit in the space between corner-shared octahedra in the 2D inorganic matrix. In Figure 3, all the previously reported conjugated ligands that form 2D perovskites are summarized and classified based on the number of aromatic rings, while "Others" represents polymeric ligands or uniquely featured ligands. Ligands with a single ring or simpler structure are not included here because of their relatively large HOMO-LUMO gaps and insulating nature (they are classified as conventional ligands and have been reviewed in numerous recent works). We suggest refs 12, 43-45 for a broader discussion of 2D perovskites and refs 27, 29, and 32 for our earlier discussion of OSiPs. Generally, ligands that can be applied to OSiPs are composed of four parts: head group, conjugated body, linker (between the head group and body), and side chains. The head group is typically a primary ammonium that has the lowest steric bulk, which forms ionic

Most of the linkers are one- or two-carbon chains. The central conjugated bodies could be various aromatic rings based on thiophene, benzene, naphthalene, heteroarenes, C-C double bond connection, etc. Side-chain modification focuses on the functionalization of any non-ammonium site including the opposite terminus in a linear ligand. 59,60,74,75 The structure of the ligand affects the packing, introduces various secondary interactions, governs the distortion of $[BX_6]^{4-}$ octahedron, and determines the feasibility of forming 2D structure. In the following section, we will briefly discuss some of the ligands and their related features in each category.

bonds with $[BX_6]^{4-}$ octahedra.

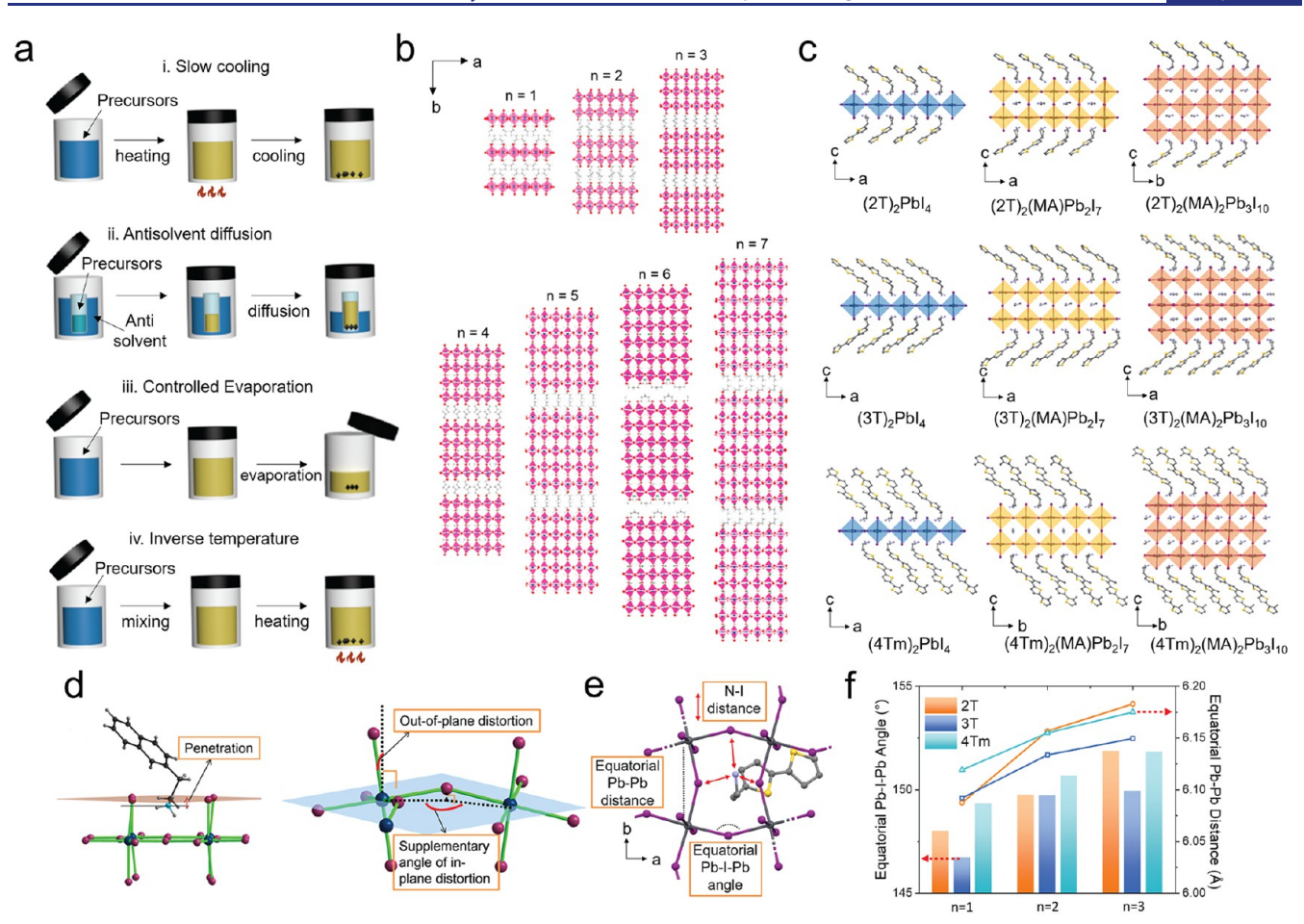


Figure 4. (a) Methods of 2D perovskite single-crystal synthesis. Adapted with permission under a Creative Commons CC-BY 4.0 license from ref 31. Copyright 2021 The Authors, published by John Wiley & Sons. (b) BA-based 2D perovskite single-crystal structures, n = 1-7. Adapted from ref 45. Copyright 2019 American Chemical Society. (c) 2T, 3T, and 4Tm-based 2D OSiPs single-crystal structures, n = 1-3. Reproduced with permission from ref 87. Copyright 2023 Springer Nature. (d) 2D perovskite single-crystal structure analysis based on NH₃ penetration and in-plane and out-of-plane distortion. Reproduced with permission from ref 24. Copyright 2017 American Chemical Society. (e) 2D perovskite single-crystal structure analysis based on parameters including N–I distance, equatorial Pb–I–Pb angle, and Pb–Pb distance. (f) Structural parameters of high-n OSiPs based on 2T, 3T, and 4Tm. Reproduced with permission from ref 87. Copyright 2023 Springer Nature.

Ligands with a two-ring structure can be obtained from one step of a carbon-carbon cross-coupling reaction or a direct modification on naphthalene. Overall, two-ring structures are synthetically simple to achieve, and the corresponding OSiPs usually adopt type I alignment. Naphthalene was incorporated into perovskite structure as early as the 1990s, with the observation of enhanced phosphorescence. 24,49 Tuning the length of the linker on naphthalene changed the penetration depths of the ammonium head and affected the distortion of inorganic layers (2-8, NMA; 2-9, NEA, etc.).²⁴ For the bithiophene-based organic ligands (2-1, 2T; 2-2, AE2T, etc.), both DJ-phase and RP-phase 2D perovskites can easily form. 28,76 Gleaned from bithiophenes, a complete set of DJphase perovskites with diammonium thiophene ranging from two to five units (AE2T to AE5T)^{18,76,77} and a series of RPphase perovskite with monoammonium thiophene extending from two to four units $(3-1, 3T; 4-2, 4Tm)^{28,34,78}$ were developed, as a longer chain length with similar cross section did not interrupt the formation of 2D perovskites. Besides thiophene backbones, biphenyl (2-10, BPMA; 2-11, PP, etc.)^{52,53} or stilbene (2-14, SA; 2-15, FSA)⁵⁴-based structures are also reported. Incorporating a photoswitchable azobenzene into a perovskite lattice is intriguing, but more fundamental

optical analysis is required to confirm the photoswitching behavior. $^{\rm 55,56}$

Further increasing the conjugation from two to three rings could lead to a solubility issue and processing difficulties in device applications. Therefore, ligands PPT (3-3) and PPT' (3-4) were designed to have methyl groups to introduce distortion and decrease the planarity between the aromatic rings, and they showed excellent performance in LED device applications. 42 Initiated with a naphthalene-based organic emitter,⁴⁹ molecular engineering of conjugated three-ring aromatics allowed photoluminescence management via doping fluorophores into 2D perovskites. For instance, Khaoula et al. observed enhanced luminescence after doping 10% NAA (3-6) into a PEA₂PbBr₄ (PEA is phenylethylammonium) 2D perovskite lattice.⁵⁷ The increased fluorescence yield was explained by the improved crystallinity or resonance between Wannier and Frenkel excitons. The same doping strategy on PEA-based 2D perovskites was also applied to 1,8-naphthalimide (3-7, NIA) and TTPhMA (3-9) for room-temperature phosphorescence via triplet-state energy transfer. 48,58,7

Based on a quaterthiophene skeleton, we recently designed and synthesized a suite of mono-ammonia ligands aiming at delicate 2D perovskite structural tuning and structureproperty relationship investigation.²⁸ Compared to the butylammonium (BA) ligand, the 4T ligand (4-1) can be considered as a counterpart that transforms each individual carbon to a thiophene ring. By adding methyl substituents to break the planar stacking, 4T can be converted to a processable version, 4Tm (4-2), with better solubility. 28 Exploiting the versatile 4Tm ligand, fundamentals like optoelectronics, ion diffusion in heterostructures, and applications including solar cells, FETs, thermoelectric devices have been demonstrated. 34,37,41 Derived from 4Tm molecules, BTm (4-3) with a 2,1,3-benzothiadiazole unit and 4TCNm (4-5) with electronwithdrawing cyano groups were synthesized. Especially, BTm revealed a narrow band gap and formed a reversed-type I alignment with $[PbI_6]^{4-.38}$ Replacing the central thiophene with thienothiophene or dithienothiophene imparted the new ligands TT (4-11) or DTT (4-12) to become highly planar structures, which allows a variety of intermolecular interactions, facilitating the nucleation kinetics.⁴⁰ Changing the central thiophene to selenophene (4-4, STm) is also synthetically feasible while the properties remain similar.³³ Adding ethyl side chains or increasing the number of methyl groups (4-6, 4Te; 4-7, 4Tdm) modulated the solubility and the lattice strain of OSiPs, which brought a macroscopic variation of surface morphology in 2D/3D perovskite heterostructures.⁵⁹ Halide functionalization (4-8, F4Tm; 4-9, Cl4Tm; 4-10, Br4Tm) was achieved on the terminal thiophenes via halogenation, allowing a fine-tuning of energy levels. 60 Other functionalities like aggregation-induced emission (4-21)⁶⁵ and donor-acceptor-donor (4-22)⁶⁶ configuration can also be integrated into the large fused ring.

Further increasing the number of aromatic rings in the ligands results in the creation of 2D OSiPs with embedded polymers. Besides the aforementioned polydiacetylene, 20,72 polymers like polythiophene,⁶⁹ polyaniline,⁶⁸ polyacety-lene,^{20,72} and polystyrene⁷¹ with ammonium groups have been reported as interconnected organic spacers in 2D perovskite lattice. Polymer-based OSiPs reveal enhanced mechanical strength and stability. However, it remains challenging to obtain polymer-based OSiP single crystals, and current studies are limited to thin films. Meanwhile, the condition used for initiating polymerization requires sophisticated control to make it compatible with less stable perovskite materials (e.g., intense heating or UV light should be avoided). Head groups composed of secondary or tertiary amine are also allowed, but the crystal structure is strongly influenced to accommodate them in the inorganic lattice. For instance, a 2D perovskite crystal structure is formed when 2TBIm (O-6) binds to the relatively small [SnI₆]⁴⁻ octahedron, while a 1D perovskite is formed as a thermodynamically stable phase when switching from Sn to Pb.³⁰ Instead of increasing the conjugated backbone, a recently reported one-ring tetrazine (O-1)-based 2D perovskite also demonstrated a type II electronic structure with suppressed photoluminescence.

2.2. 2D OSiP Synthesis. 2.2.1. n = 1 2D OSiP Crystal Growth. While different conjugated ligands with varying molecular structures have been designed, it is imperative to verify how these conjugated ligands are structurally incorporated into 2D perovskites. It is necessary to acquire crucial information about how variations in these organic moieties can affect the active inorganic layers in between, leading to alterations in the semiconducting and optoelectronic properties of 2D perovskites. Thus, resolving the single-crystal structure of 2D perovskites is an important first step in terms

of defining how incorporation of conjugated ligands can ultimately lead to desirable properties. There are many different methods to obtain single crystals with varying qualities and sizes, from atomically thin nanocrystals to millimeter-scale bulk crystals. Depending on the purpose of the crystal synthesis, the crystallization means can be carefully chosen. As facile synthesis of nanocrystals maybe preferred for heterostructure construction or thickness-dependent analysis due to their uniform shapes and ultrathin nature, bulk single-crystal synthesis with longer growth duration may be suitable for single-crystal X-ray diffraction analysis or other processes that may require higher crystallinity.

Figure 4a illustrates four widely utilized methods to realize high-quality 2D perovskite bulk single crystals. The commonality between them is the use of the solubility difference across different temperatures or solvent compositions. Slow-cooling crystallization is the most universal as well as the earliest used method, being employed in the beginning stages of investigations regarding 2D perovskite crystals carried out by Mitzi et al. in the mid-1990s. §0,81 This method involves the use of concentrated aqueous hydroiodic acid solutions of precursors that are typically LX/LX2 and BX2 for a 2D perovskite with a formula of L₂BX₄ or LBX₄. In aqueous acidic solutions, 2D perovskites usually possess a solubility curve which increases with higher temperature. Thus, the general process initially involves dissolving all the precursors in solution with sufficient heating until it becomes a transparent yellow solution. Then, the solution is slowly cooled at an appropriate rate through an oil bath or a Dewar flask until it reaches room temperature, yielding high-quality bulk single

However, due to the acidic and aqueous nature of the solvent system, the slow-cooling method poses a challenge for incorporating conjugated ligands, which are relatively less soluble in aqueous solution compared to conventionally utilized organic moieties. Thus, antisolvent diffusion crystallization provides another solution to incorporate conjugated ligands into 2D perovskite single crystals. This method takes advantage of the change in the solubility of 2D perovskites with respect to the shift in the composition of organic solvents. N,N-Dimethylformamide (DMF), dimethyl sulfoxide (DMSO), and γ -butyrolactone (GBL) are typically used as good solvents, while chlorobenzene, diethyl ether, and toluene are chosen as antisolvents. As demonstrated by Tian et al., this general method involves the dissolution of the precursors in a small vial which is inserted into a bigger vial filled with an antisolvent.⁸² With time, the antisolvent vapor diffuses into the smaller vial, triggering the precipitation of 2D perovskite crystals once the solution reaches a supersaturated state, as shown in Figure 4a.

Besides the two methods mentioned above, crystallization through controlled evaporation has also been used to realize (PEA)₂PbBr₄ crystals, as demonstrated by Zhang et al. ⁸³ This process requires careful control of the evaporation speed to limit the extent of nucleation as well as maintain prolonged growth of single crystals to realize millimeter-scale crystals. Lastly, inverse-temperature crystallization utilizing solvent systems that possess decreasing solubility with higher temperature has also been employed by Liu et al. to synthesize high-quality single crystals of (PEA)₂PbI₄. ⁸⁴ Both methods are illustrated in Figure 4a and typically involve the use of organic solvents, unlike the slow-cooling method.

2.2.2. High-n-Number 2D OSiPs' Growth and Properties. Although multiple previous studies have successfully produced high-quality crystals of n = 1 2D perovskites utilizing the four methods mentioned above, the high-n-number 2D (or "quasi-2D") perovskite growth method has been limited mostly to slow-cooling crystallization. Starting from n = 1-4 BA-based 2D perovskite structures reported by Stoumpos et al., the field has been able to resolve the single-crystal structures of 2D perovskites up to n = 7, with the composition of $(BA)_2(MA)_6$ -Pb₇I₂₂, using the slow-cooling method reported by Mao et al. 85,86 Figure 4b shows all the resolved single-crystal structures of 2D perovskites incorporating BA ligand from n = 1 to 7.⁴⁵ Incorporating conjugated ligands into high-n 2D perovskites has been considered a great challenge due to the limited solubility of conjugated ligand precursors in aqueous acidic solution, which is required for high-n-number crystallization. To overcome this challenge, Park et al. was able to devise a new solution system that incorporates alcoholic solvents to modulate the overall polarity of the crystallization conditions, aiding in the dissolution of precursors as well as helping the growth process of single crystals.⁸⁷ With careful control of the alcoholic solvent composition depending on the extent of hydrophobicity the incorporated conjugated ligands possess, they were able to successfully obtain the single-crystal structures of 2D OSiPs incorporating 2T, 3T, and 4Tm with n from 1 to 3, as shown in Figure 4c.

Resolving single-crystal structures is just a starting point for defining the structure-property relationship in 2D perovskites. Understanding the effect of organic cations, especially conjugated ligands, on the overall structure, especially the inorganic part, is critical considering the hybrid nature of 2D perovskites. As reported by Du et al., it is evident that the extent of organic cation penetration can greatly alter the inplane and out-of-plane distortion among the inorganic octahedra sandwiched between the two organic layers (Figure 4d).²⁴ Figure 4e summarizes important parameters describing the perovskite lattice and the organic cations, such as N-I distance (parameter for organic cation penetration), equatorial Pb-I-Pb angle, and Pb-Pb distance (parameter for in-plane distortion). The Pb-I-Pb bond angle, as shown in Figure 4e, is a structural indicator for distortion and is heavily influenced by the NH₃ penetration into the inorganic octahedral plane. For the organic ligands incorporated in n = 1 2D perovskites, BA and PEA show relatively low organic cation penetration. Incorporating conjugated ligands greatly decreases the N-I distance, signaling considerable protrusion of the organic moieties into the inorganic layer. With more organic cation penetration, the octahedral tilting in the inorganic slabs increases. This trend shows the evident effect of conjugated ligand designs on the overall structural rigidity as well as distortion. With increasing *n*-number (Figure 4f), the structural parameters approach those of their 3D counterparts, with less distortion of the inorganic layer. With simultaneous modulation of molecular design and dimensionality (n-number) in 2D perovskites, precise structural characteristics can be achieved which may further translate into desirable properties stemming from well-defined structure-property relationships.

2.2.3. Ligands That Cannot Form 2D Perovskites. As stated, growing single crystals of 2D perovskites and resolving the complete single-crystal structure can be challenging, as the size of the crystals is small and their quality is always affected by structural twinning, defects, and lattice softness. In addition, the presence of bulky organic ligands in OSiPs makes single-

crystal cultivation even more difficult compared to other small ligands. For example, the perovskite structure with fullerene derivatives (O-8) has not yet been confirmed by single-crystal X-ray diffraction. Only thin-film properties suggested the formation of this OSiP.73 Instead of forming the desired layered 2D perovskite structure, the formation of 1D chains or 0D clusters is sometimes inevitable. 88-91 With regard to the assembly of 1D versus 2D perovskite structures, Tremblay et al. discussed 16 phenyl-ligand-based perovskite crystal structures. 92 They proposed that the formation of either intramolecular hydrogen bonding between the ammonium and substituents on rings or intermolecular hydrogen bonding between neighboring ammoniums drives the structure toward 1D face-shared $[PbI_6]^{4-}$ chains. When ammonium solely interacts strongly with the $[PbI_6]^{4-}$ octahedra, the 2D perovskite structure is typically favored. Furthermore, the preference of forming 2D or 1D structures is also hard to computationally predict. Despite the simulation predictions of the large NDIC2 ligand (Figure 5a) exhibiting a stable 2D

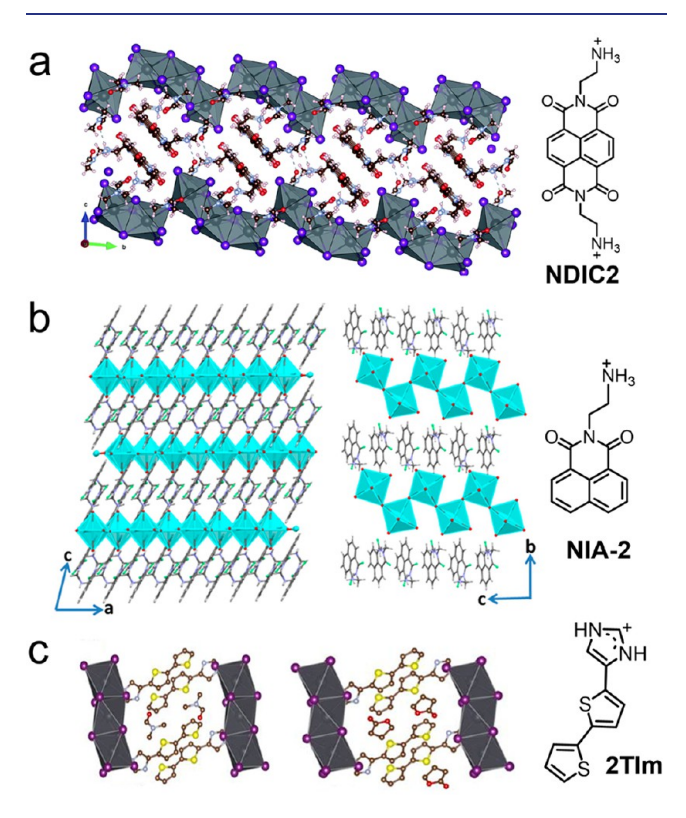


Figure 5. Representative 1D perovskites that incorporate conjugated ligands. (a) Single-crystal structure of (NDIC₂)Pb₂I₆. Reproduced with permission from ref 94. Copyright 2021 Royal Society of Chemistry. (b) Single-crystal structure of (NIA-2)BiI₅. Reproduced with permission from ref 95. Copyright 2020 American Chemical Society. (c) Single-crystal structure of (2TIm)PbI₃·(DMF or GBL). Reproduced with permission from ref 30. Copyright 2022 John Wiley and Sons.

perovskite structure of (NDIC2)PbI₄, the resulting crystals were discovered to be 1D-chain structures or 0D clusters with isolated [Pb₅I₁₆]⁶⁻ octahedra under varying conditions.^{63,93} Interestingly, one of the 1D structures with (NDIC2)Pb2I6 formula forms a type II band alignment because the LUMO of NDIC2 is lower than the CBM of $[Pb_2I_6]^{2-.94}$ Pious et al. also reported type II band alignment based on naphthalimide

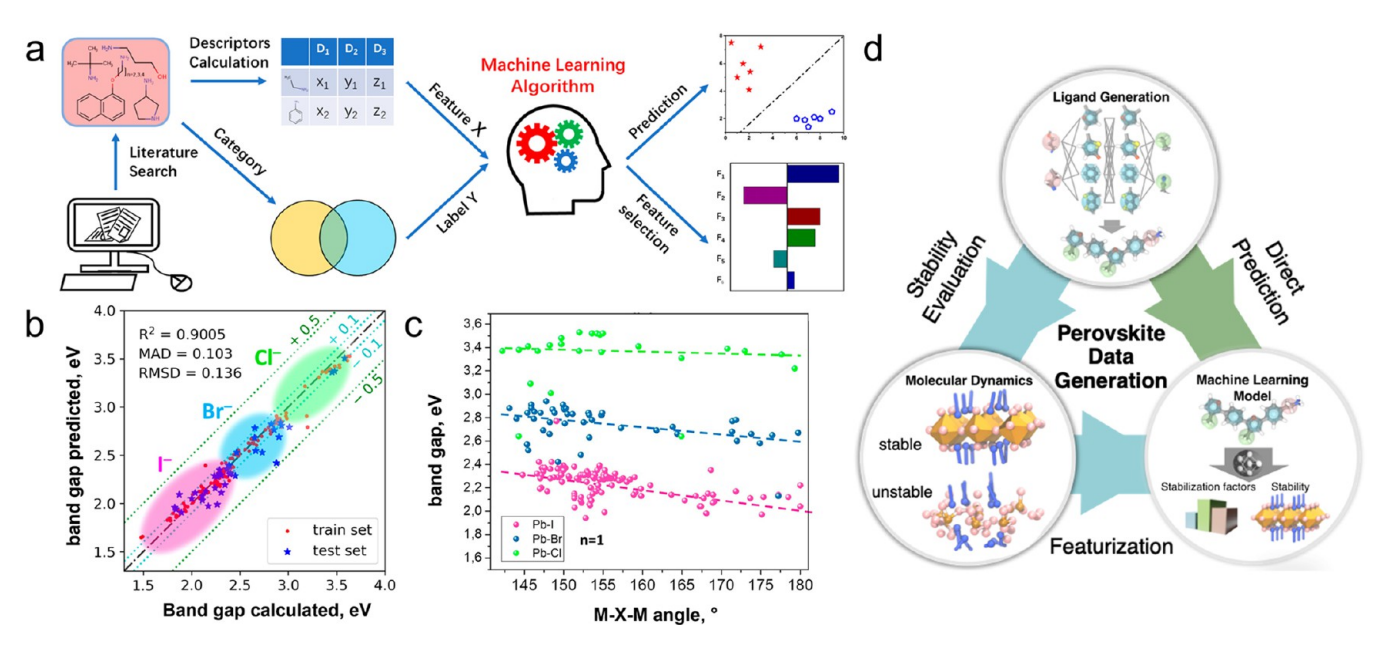


Figure 6. (a) Workflow of machine-learning-assisted exploration. Reproduced with permission from ref 102. Copyright 2021 American Chemical Society. (b) Band gaps of 2D hybrid halide perovskites calculated by density functional theory and predicted by the ML model. (c) Correlation between band gap and metal-X-metal angle. Reproduced with permission from ref 111. Copyright 2020 American Chemical Society. (d) Molecular dynamics simulation approaches for ligand-perovskite stability prediction. Reprinted with permission under a Creative Commons CC-BY license from ref 116. Copyright 2023 The Authors, published by John Wiley and Sons.

(NIA-2) with strong $\pi - \pi$ interaction inserted into the bismuth-based zigzag octahedra (Figure 5b).95 Wudl et al. first reported the tetrathiafulvalene (TTF) components and discovered the radical cation state of TTF in the (TTF)Pb2I5 hybrid structure with semiconducting properties. 96,97 Our group initiated the use of nontraditional formamidinium, imidazolium, and benzimidazolium as the head groups of conjugated ligands to form OSiPs. 30 But we found that the 2D perovskite is weakly crystallized, and 1D perovskite crystals often occur because the size of the head group is too large to accommodate. New ligands such as 2TImI, with an imidazole head group (Figure 5c), form a face-sharing [PbI₆]⁴⁻ chain structure with the inclusion of solvent. Compared to 2D perovskite, 1D/0D perovskite provides a perfect scaffold for the study of broadband emission with self-trapped excitons, enabling the study of transfer kinetics, conductivity, and aqueous stability, 89 as well as light-emitting device applications with high photoluminescence quantum yield. 98-100 Clearly, a vast chemical design space exists for the 0D and 1D hybrids, as both inorganic and organic components can be manipulated. However, due to the lack of electronic coupling in a second or third dimension, the charge transport properties of these materials are usually inferior to those of 2D or 3D perovskite materials.

2.3. Computational Prediction of 2D Perovskites. An exciting aspect of 2D perovskites is their tunability due to the relatively permissive size restrictions on organic ligands capable of fitting within the lattice. Contrary to their 3D counterparts, whose A-site cation size is subjected to the Goldschmidt tolerance factor, 101 to date, there are no definite rules established on the size of the ligands in 2D perovskites except that they cannot be too bulky to fit in the inorganic lattice or too small, as that would favor the formation of other dimension perovskites. 12 Since the ligands relevant to OSiPs tend to be large, it is critical to know the 2D perovskites' structural information before spending tremendous efforts in

their synthesis. So far, there are only some empirical observations of the factors that are conducive to 2D perovskite formation: (1) The intramolecular hydrogen bonding of ammonium can increase the size of the head group, which makes the 2D structure less favorable. 92,102 Conversely, it is also reported that the intramolecular hydrogen bonding can stabilize 2D perovskites by shortening the ammonium penetration depth. 51,103 (2) If the linker length is too short, steric hindrance between the large conjugated moieties of the OSiP ligand and the inorganic sheet disfavors 2D perovskite formation. (3) The cross section of the ligand matters since 2D perovskites are relaxed in the out-of-plane direction. The inplane structure still requires a small cross section to fit in the "pocket" of $[BX_6]^{4-}$ octahedra. Overall, despite continuous experimental efforts in exploring new ligand designs for the spacer cations, the number of synthesized structures is small compared to the immense design space of OSiPs. This lack of exploration creates opportunities to improve the understanding of structure-property relationships, the aspects of organic ligands that select for 2D-phase formation, and the ultimate limits of ligand-tuned perovskite properties. Apart from a few structural features, including metal-halide bond length and spacer length, that have been revealed to be related to the band gap, light harvesting, and device efficiency by experimental research, most structural features remain unidentified. 104,105

Although machine learning (ML) has been adopted for property prediction in many chemical design applications, 106-109 the lack of significant datasets has limited the lack of significant datasets has limited applications for 2D perovskites. Nevertheless, simpler ML models like random forests and support vector machines (SVMs) have been used to show how ligand features influence some properties. Wu and co-workers trained SVMs with an experimental dataset of ligands (<100 from reported structures) to predict the reactivity between amine passivators and perovskites and the dimensionality of low-dimensional Pb-I perovskites (Figure 6a). 102,110 The models revealed that

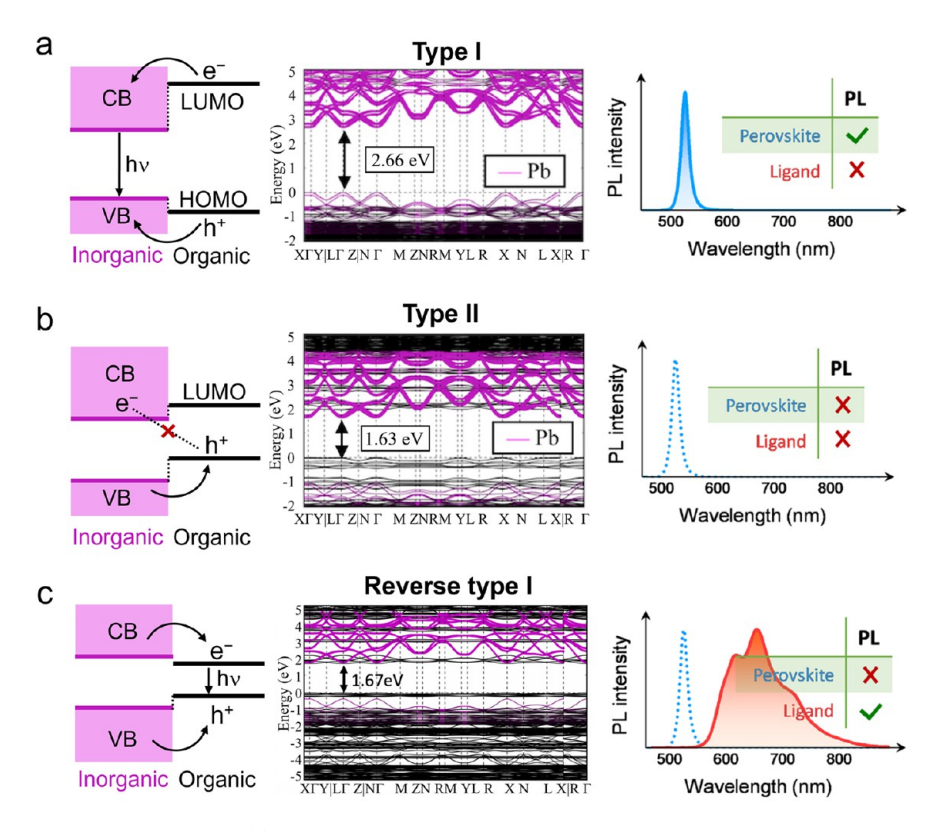


Figure 7. Optoelectronic properties of OSiPs. (a) Energy scheme of a type I alignment, band structure of (AE1T)PbBr₄ 2D perovskite, and photoluminescence of (2T)₂PbI₄ 2D perovskite. (b) Energy scheme of a type II alignment, band structure of AE5TPbBr₄ 2D perovskite, and photoluminescence quenching of (4Tm)₂PbI₄ 2D perovskite. Reproduced with permission from ref 17. Copyright 2018 American Physical Society. (c) Energy scheme of a reverse type I alignment, band structure of (BTm)₂PbI₄, and photoluminescence of (BTm)₂PbI₄ 2D perovskite. Adapted with permission from ref 28. Copyright 2019 Springer Nature. Reproduced with permission from ref 160. Copyright 2021 The American Association for the Advancement of Science.

the steric environment around the nitrogen atom (steric effect index), the H-donor count, the number of substituents on the nitrogen atom, and branched isomers are the important features in determining the amine's reactivity with the MAPbI₃ perovskite film out of 31 tested features. As for dimensionality prediction, the steric effect index, eccentricity, largest ring size, and H-donor count were identified as important features. A model based on these features to predict the odds of forming 2D perovskites achieved a 79% accuracy. Marchenko et al. built a database of experimentally investigated 2D perovskites, which included 515 known compounds containing 180 different organic cations, 10 metals (Pb, Sn, Bi, Cd, Cu, Fe, Ge, Mn, Pd, and Sb), and 3 halogens (I, Br, and Cl). 111 Their database was used to train a supervised ML model to predict band gaps. The model achieved accuracy within 0.1 eV and revealed that the predicted values of band gaps decrease with increasing metal-X-metal angles (Figure 6b,c). Despite the pioneering nature of these efforts, the chemical scope for training and validating these models was narrow and cannot be used at this point to elucidate the more general design relationships of 2D perovskites. In contrast, several ML models have been successfully trained to accelerate the finding of new 3D halide perovskites. Deep learning models, classical ML models, as well as a high-throughput screening frameworks have been developed to predict various electronic properties and aid ligand design with well-discovered features. 112-115 Lin et al. recently published a molecular dynamics (MD) simulation study of over 10k prospective OSiPs to establish design rules for stable ligand incorporation (Figure 6d). 116

Due to the ability of the ligands to relax across unit cells, they found that ligands larger than the unit cell along one dimension can still be accommodated in many cases and that linker selection plays a critical role for several specific body chemistries. These predictions were also experimentally validated by the synthesis of novel ligands and the formation of 2D perovskites.

2.4. 2D OSiP Structure—Property Relationships. 2.4.1. Optoelectronic Properties. 2D perovskites are considered intrinsic quantum wells, in which the inorganic wells are separated by organic barriers with low dielectric constant at a molecular scale. 117,118 Therefore, the effective band gap can exceed 2.5 eV, and the exciton binding energy increases to more than 400 meV in Pb-based halide perovskites, due to the quantum and dielectric confinement effects. 119-121 Increasing the *n*-number of 2D perovskites (as "quasi-2D") increases the well thickness and decreases the band gap. Intrinsically, the metal center with different electronic band structures contributes significantly to the band structure; for example, Pb-based perovskite has a larger band gap compared with Snbased perovskite. 122 The halides from Cl to Br to I with hybridized p orbitals make the VBM shallower, and therefore the band gap follows the trend of Cl > Br > I.¹⁷ Differently, OSiP organic spacers with increased conjugation can provide interband frontier orbitals, decrease the difference of dielectric constant, and indirectly affect the band gap via lattice distortion. In Figure 7a, we use AE1T molecules and 2T (2-1) ligand to demonstrate a typical type I band structure, and photoluminescence arises from the excitons confined within

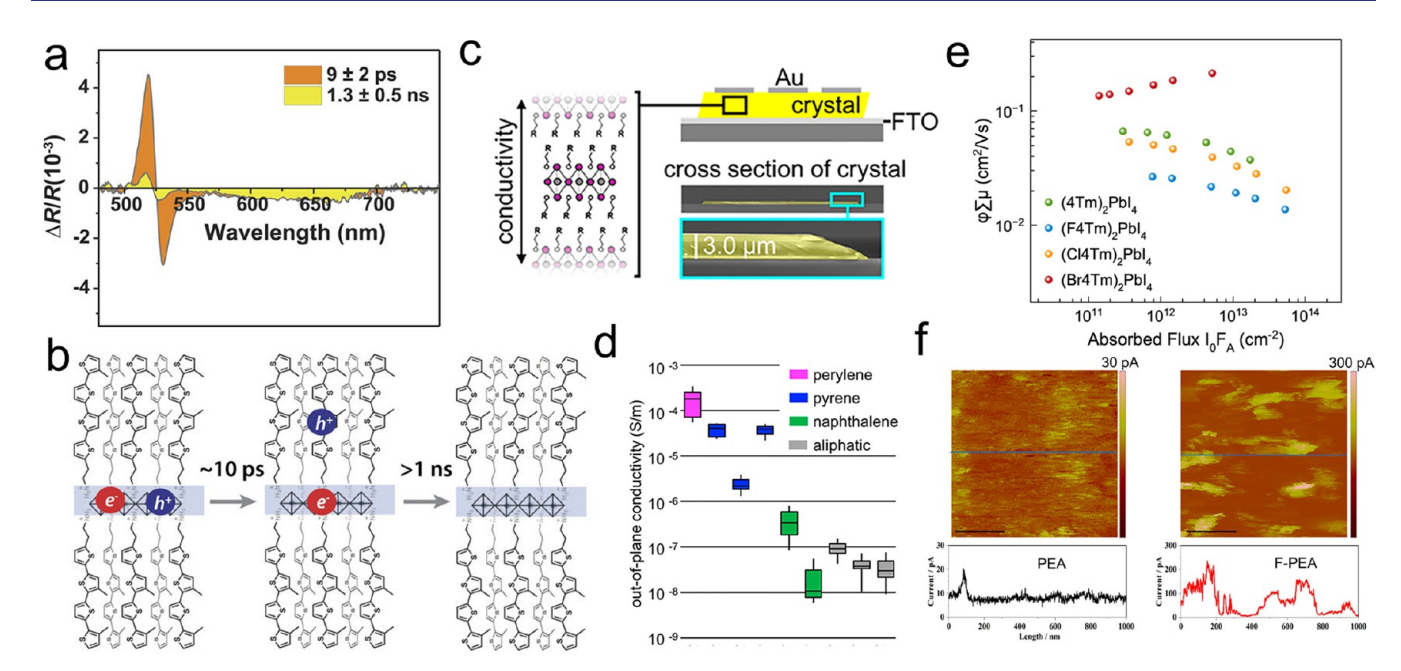


Figure 8. Carrier dynamics and transport of OSiPs. (a) Decay-associated spectra of $(4Tm)_2PbI_4$, based on global analysis of the transient reflection spectra. (b) Schematics of charge separation and recombination of $(4Tm)_2PbI_4$. Reproduced with permission from ref 123. Copyright 2020 AIP Publishing. (c) Out-of-plane conductivity measurement on 2D perovskite single crystals. (d) Comparison of the out-of-plane conductivity among various organic cations. Reproduced with permission from ref 51. Copyright 2018 American Chemical Society. (e) Time-resolved microwave conductivity measurement of 4Tm, F4Tm, Cl4Tm, and Br4Tm 2D perovskites. Reproduced with permission under a Creative Commons CC-BY 4.0 license from ref 60. Copyright 2023 The Authors, published by the American Association for the Advancement of Science. (f) Conductive atomic force microscopy of 2D perovskite films based on F-PEA and PEA (n = 5). Reproduced from ref 127. Copyright 2019 American Chemical Society.

inorganic layers. The organic part, with a large band gap, does not influence the photoluminescence. In Figure 7b, AE5T and 4Tm (4-2) represent a typical type II band alignment, in which the HOMO of the organic moieties is above the VBM of the inorganic lattice or the LUMO of the organic moieties is below the CBM, resulting in a staggered configuration. Charge extraction can occur within the molecular scale of the inorganic-organic interface with this type II energy alignment, causing quenched photoluminescence. In Figure 7c, ligand BTm (4-3) has been demonstrated to form a reversed-type I alignment, in which the LUMO is below the CBM and the HOMO is above the VBM. Therefore, in this case, only the organic part contributes to the broad photoluminescence, with fast energy and/or charge transfer from the inorganic lattice. So far, to the best of our knowledge, only (BTm)₂PbI₄ and (AE4T)PbCl₄ have been reported to possess reversed-type I alignment. 18,28 OSiPs with a tunable quantum-well-like alternating structure, whose band structure has been simulated based on density functional theory including spin-orbit coupling adjustment, were established by the Blum group, and the results showed good agreement with experimentally observed optoelectronic properties. 17

2.4.2. Carrier Dynamics and Transport. Different types of band alignment and steady-state optical properties lead to differences in the charge separation, recombination, and energy-transfer dynamics of OSiP materials, according to time-resolved spectroscopy studies. ¹²³ As shown in Figure 8a, (4Tm)₂PbI₄ reveals a bleach peak around 515 nm from excitonic absorption. Based on the decay-associated spectra, the time scale of excitonic decay is around 10 ps, which is shorter than that of (BA)₂PbI₄ with a wide-band-gap BA ligand, suggesting fast hole extraction from [PbI₆]⁴⁻ octahedra

to the 4Tm ligand (4-2). Moreover, the decay of the chargeseparated state in (4Tm)₂PbI₄ is observed to be longer than 1 ns (Figure 8b), demonstrating efficient interfacial charge transfer and a long-lived charge-separated state in 2D OSiPs. 2D halide perovskites also exhibit anisotropic charge transport. Typically, the in-plane conductivity with continuous inorganic sheets is higher than that of the out-of-plane direction which is composed of insulating organic barriers. 124,125 In addition, increasing the number of inorganic layers will enhance the conductivity because of the decreased ratio of organic constituents. Stupp and co-workers first studied the out-ofplane conductivity on the 2D perovskite single crystals incorporating large aromatic ligands (Figure 8c,d).⁵¹ Due to the better energy alignment with the inorganic framework, the as-formed 2D perovskites with perylene and pyrene revealed higher out-of-plane conductivity compared to perovskites with aliphatic spacers. In terms of the in-plane direction, polydiacetylenes with in-plane conjugation networks have been demonstrated to significantly increase the conductivity. Besides the I-V diode measurement that required electrodes as current collectors, a contactless time-resolved microwave conductivity measurement is widely used in 2D perovskite to study the carrier transport. $^{126-129}$ Combining the single-crystal analysis and microwave conductivity measurement, it was found that the Br4Tm ligand (4-10) with better organic layer packing in crystal structures exhibited the highest conductivity among all halogen-4Tms (Figure 8e).60 Conductive atomic force microscopy is another technique that allows the mapping of surface conductivity. 130 As shown in Figure 8f, the 4fluorophenethylamine (F-PEA)-based 2D perovskite with parallel slip-stacking has 10-fold higher conductivity than PEA-based 2D perovskite with an edge-to-face packing.¹

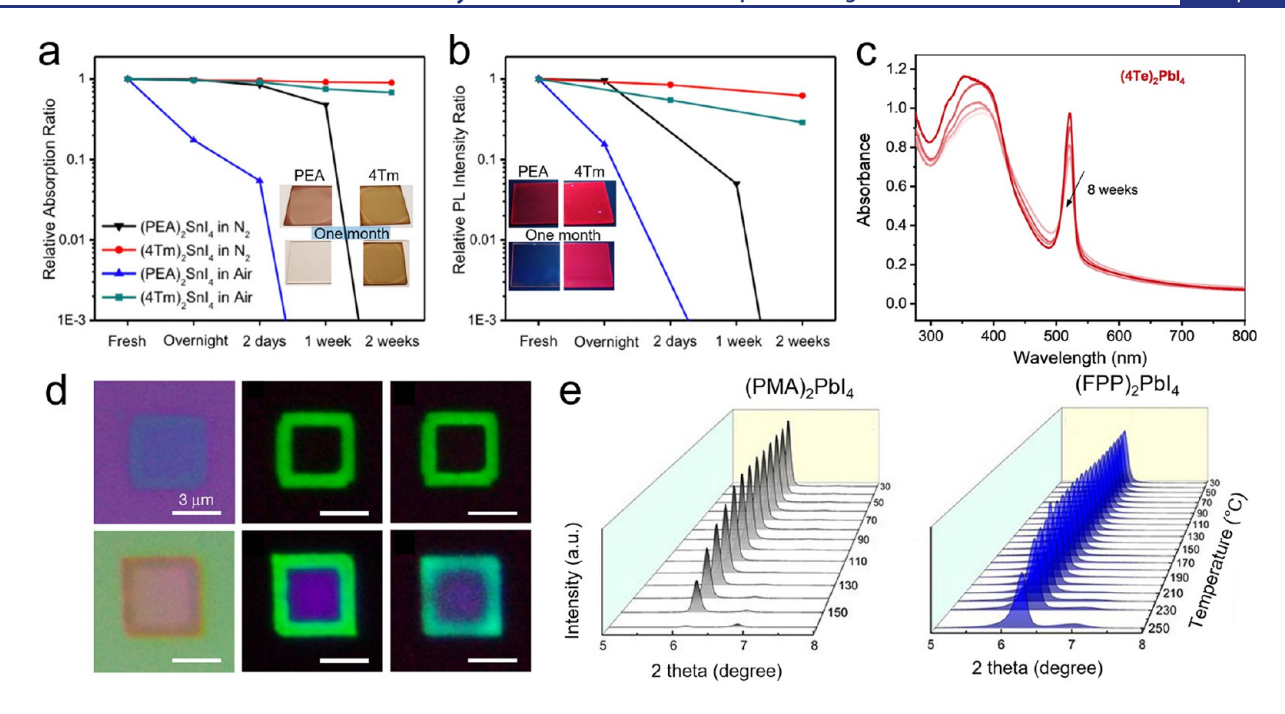


Figure 9. Stability of OSiPs. (a) Absorption changes of (PEA)₂SnI₄ and (4Tm)₂SnI₄ films upon storage in air or N₂. Insets are pictures of the films before (top) and after (bottom) storage in air for 1 month under daylight. (b) Photoluminescence changes of (PEA)₂SnI₄ and (4Tm)₂SnI₄ films upon storage in air or N₂. Insets are pictures of the films before (top) and after (bottom) storage in air for 1 month under UV light. Adapted from ref 34. Copyright 2019 American Chemical Society. (c) Absorption changes of (4Te)₂PbI₄ films upon water immersion. Reproduced with permission under a Creative Commons CC-BY 4.0 license from ref 59. Copyright 2023 The Authors, published by John Wiley and Sons. (d) Optical and photoluminescence images of a (2T)₂PbI₄-(2T)₂PbBr₄ and a (BA)₂PbI₄-(BA)₂PbBr₄ lateral heterostructure. Reproduced with permission from ref 78. Copyright 2020 Springer Nature. (e) Temperature-dependent X-ray diffraction patterns of PMA and FPP 2D perovskites. Reproduced with permission from ref 53. Copyright 2021 American Chemical Society.

2.4.3. Stability. The moisture and thermal stabilities of 2D perovskites are better than those of 3D perovskites due to the organic spacers being bulkier and more hydrophobic than MA and FA cations, leading to suppressed ion migration across the organic barriers. OSiPs with typically longer conjugated bodies can further enhance the moisture stability. In other words, the use of bulky organic cations in OSiPs can be seen as a natural addition to protective encapsulation layers. As shown in Figure 9a,b, compared to PEA₂SnI₄, which degrades within 1 day, (4Tm)₂SnI₄ has its absorbance and photoluminescence retained in air for up to 2 weeks. Accordingly, a (4Tm)₂SnI₄-based FET device has its hole mobility largely retained in air for up to 1 month, significantly ameliorating the oxidation and hydrolysis problem of Sn-based perovskites. 34,131 For lead-based OSiPs, the moisture stability can be monitored by directly immersing thin films in water. Taking advantage of its hydrophobic ethyl side chains, (4Te)₂PbI₄ was reported to have excellent aqueous stability, and the films were stable even after 8 weeks of water soaking (Figure 9c).⁵⁹ Constructing heterostructures offers another approach to study and analyze the thermal stability of 2D perovskites (Figure 9d). 78,132,133 The degradation of 2D perovskites originated from their "soft" lattice, which allows anion diffusion. In the lateral heterostructures of $(2T)_2PbI_4-(2T)_2PbBr_4$, where the $(2T)_2PbI_4$ has green emission and the (2T)₂PbBr₄ has its emission quenched, no obvious interdiffusion of anions (I and Br) was observed after heating. However, in the (BA)₂PbI₄-(BA)₂PbBr₄ lateral structure, where (BA)₂PbI₄ has green emission and the central (BA)₂PbBr₄ has blue emission, obvious blurriness can be observed at the boundary after heating, accompanying a significant change in the emission spectra. The anionic

diffusion has been quantified in both epitaxial and lateral heterostructures of 2D halide perovskites. ^{132,133} Therefore, the anion diffusion is better inhibited using bulky organic cations, while the increase in the *n*-number of 2D perovskites can promote the anion diffusion. Zhao et al. studied the thermal stability of diammonium ligands that form DJ-phase 2D perovskite (Figure 9e) and observed from the temperaturedependent X-ray diffraction patterns that the DJ-phase 2D perovskite incorporating biphenyl diamines has better stability than the RP-phase counterpart with single-ring phenylmethylammonium (PMA) cations.⁵³ Fluorination of the diammonium ligand (2-12, FPP) can further enhance the thermal stability by improving crystallinity, while polymerization of the 4-vinylbenzylammonium (O-5, PVBA) forms 2D perovskites with interconnected ligand 2D layers, enhancing the overall rigidity and stability, evident from temperature-dependent photoluminescence spectra and water soaking tests.⁷

3. DEVICE APPLICATIONS OF OSIPs

3.1. Application in Solar Cells. Due to the impressive stability of 2D perovskites against ion migration and ambient environment, this type of material has been adopted in the structure of PSCs to address stability issues, either in replacement of 3D perovskites or in combination with 3D perovskites (Figure 10a). To address the charge-transfer issues caused by incorporating organic molecules into the structure, conjugated organic ligands recently have gained increased interest. However, translating the OSiP concept from fundamental studies into thin-film solar cell applications requires decent adaptation and is still in its infancy stage. 44

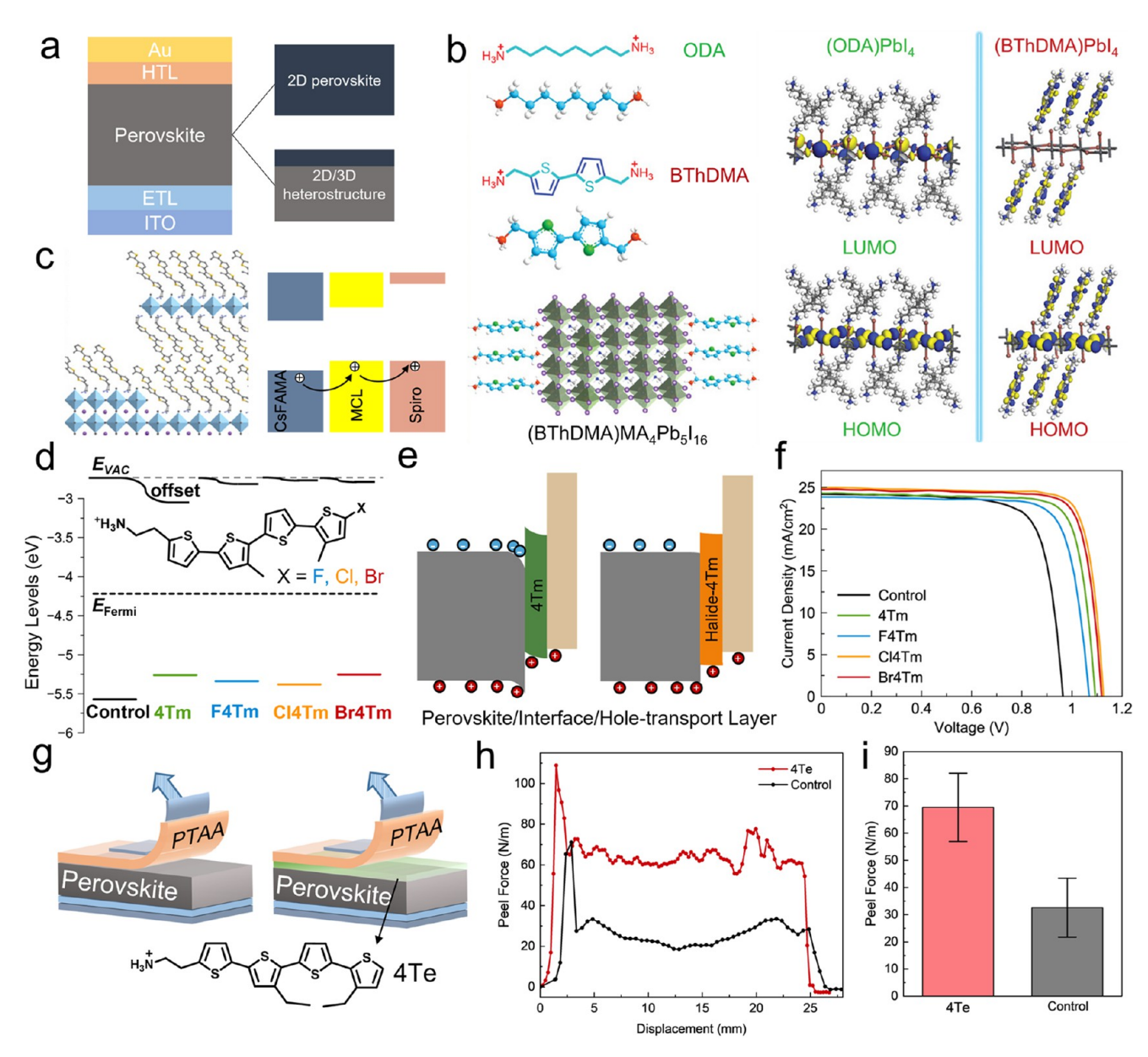


Figure 10. OSiP-based solar cells. (a) Scheme of OSiPs incorporated in PSCs. (b) Left panel: chemical structures of organic ligands and schematic crystal structure of 2D DJ perovskite. Right panel: HOMO and LUMO of the optimized 2D perovskites. Reproduced with permission from ref 47. Copyright 2023 John Wiley and Sons. (c) Structure of the 2D/3D heterojunction containing a 4Tm ligand and the energy level scheme for efficient charge transfer. Reproduced with permission from ref 41. Copyright 2023 John Wiley and Sons. (d) Energy level diagram of 4Tm and X4Tm 2D/3D heterojunction, extracted from ultraviolet photoelectron spectroscopy; inset is the molecular structure of X4Tm, X = F, Cl, Br. Adapted with permission under a Creative Commons CC-BY 4.0 license from ref 60. Copyright 2023 The Authors, published by the American Association for the Advancement of Science. (e) Illustration of interface band alignment with band bending and charge transfer. (f) Current density—voltage characteristics of pristine and ligand-2D-passivated PSCs. (g) Schematics and (h) results of 90° peel tests performed on perovskite/PTAA thin-film samples with or without 4Te-2D. (i) Statistics of peeling tests for the 4Te and control samples. Adapted with permission under a Creative Commons CC-BY 4.0 license from ref 59. Copyright 2023 The Authors, published by John Wiley and Sons.

The application of 2D perovskite in solar cells as light-absorbing materials demands not only efficient charge transfer but also desirable light absorption. To reduce the exciton binding energy and increase the absorption spectrum range, quasi-2D perovskites (n > 1) are normally employed in solar cell devices, which also applies to the perovskites incorporating conjugated ligands. Because there are already many reviews discussing the strategy of controlling the orientation and phase-purity of 2D and quasi-2D perovskite films based on wide-band-gap ligands to improve the solar cell efficiency, 43,44 we only focus on thin-film growth of perovskites incorporating

conjugated ligands. The characteristic features of these ligands are their aromatic rings and a more rigid molecular packing compared with aliphatic ligands. Adopting the concept of molecular packing in organic semiconductor crystals, the controllable packing of these aromatic molecules has initiated the study of efficient charge transfers, modulated by the fluorination of PEA.¹²⁷ It has been further demonstrated that the molecular configuration of F-PEA can influence the crystallization process, determining the phase and orientation of 2D perovskite thin films and subsequently impacting the photovoltaic device performance.¹³⁴ As aforementioned, more

comprehensive aromatic moieties including naphthalene, pyrene, and perylene have also been adopted in the formation of 2D PSCs to achieve enhanced out-of-plane conductivity due to both ligand packing geometry and reduced energy level offset between organic moieties and inorganic layers.⁵¹ However, because of the intrinsically high exciton binding energy of n = 1 2D perovskites, the as-fabricated solar cell device with a PCE of 1.38% only acted as a proof-of-concept demonstration. More recently, the conjugated ligands have been developed from benzene to electron-rich thiophene rings, and from RP phase to DJ phase. 35,47,135 The sulfur atoms in thiophene promote more delocalized valence π electrons, resulting in higher charge mobility, which is a commonly used strategy in organic semiconductors. The obvious orbital coupling between thiophene and inorganic layers hence enables the organic moieties to actively modulate the band structure of halide perovskite and facilitates efficient charge transfer between inorganic sheets. The DJ-phase perovskites, which feature bidentate bithiophene (2-4, BThDMA) bridging the inorganic sheets as conducting wire, have been shown to deliver high-PCE solar cell devices (Figure 10b).⁴⁷

With the increase of the length of conjugated ligands, the charge-transfer distance between the inorganic sheets will increase, while the differences of the dielectric constants between inorganic sheets and organic moieties will decrease. Therefore, understanding the charge-transfer mechanism and balancing the charge-transfer distance and energy barriers will require more efforts in the future to unveil the principle of building high-efficiency 2D PSCs with conjugated ligands.³⁹ However, to construct the relationship of structure-property performance, the quality of the thin films fabricated through spin-coating needs to be considered, as the crystallinity, orientation, and phase-purity are still key parameters for solar cells. The increased conjugated length of the ligands will result in the altered processability and ligand interactions from conventional ligands. Currently, the modular nucleation and growth process through solvent engineering allows control of orientation and phase distribution of 2D perovskite thin films with bithiophene ligands (2-1, 2T), although further efforts will be needed to realize absolute control over more complicated ligands.³⁵

Besides employing 2D perovskites as pure light-absorbing materials, the construction of 2D/3D heterojunctions has shown greater potential in fabricating efficient and stable PSCs. 126,136,137 The principles of conjugated ligand design, which have been applied to 2D PSCs, can also be adopted in the fabrication of advanced 2D/3D heterostructures to generate efficient devices. However, the newly generated interfaces between 2D and 3D perovskites require proper energy level alignment and interfacial geometric contact to support charge transfer across the interfaces. Construction of an interfacial dipole has been demonstrated through the design of a conjugated aniline ligand to improve the energy alignment and substantially deliver high-efficiency devices. 138 The lowdimensional structure can be extended from 2D to 1D, as some innovative conjugated ligands cannot form stable 2D perovskites. 139 However, to fully retain the potential of conjugated ligands in 2D/3D heterojunctions, further tuning of the band structure of conjugated ligands through molecular configuration to achieve controlled 2D/3D energy alignment is required. It had been demonstrated that, with the small-bandgap conjugated ligand 4Tm (4-2), which forms type II energy alignment with the inorganic sheet in a 2D perovskite, the 2D

capping layers on the 3D surface can increase the VBM of the 3D perovskite surface and facilitate efficient hole extraction (Figure 10c). To further reduce the energy level offset between ligand and inorganic sheets in 2D perovskites, halogen-4Tm ligands (4-8 to 4-10) were designed and synthesized in a more recent study (Figure 10d, inset). Extracted from ultraviolet photoelectron spectroscopy, Cl4Tm (4-9) reveals the smallest band-bending at the interface between the perovskite and hole-transport layer, showing efficient hole extraction and less electron accumulation (Figure 10d-f). Combined with significantly improved out-of-plane conductivity, Cl4Tm-based PSCs delivered a champion efficiency of 24.6%, demonstrating the highest performance among poly(triarylamine) (PTAA)-based n-i-p PSCs.

In terms of interface contact, the 2D OSiP interlayer composed of side-chain-modified 4Te ligands (4-6) improved the interfacial adhesion with the PTAA hole-transporting layer. ⁵⁹ Mechanical peel tests showed that 4Te passivation with conformal 2D/3D heterostructures exhibited twice the peel force, which is attributed to enhanced π - π interactions between conjugated ligands and aryl-based PTAA (Figure 10g-i). The perovskite devices employing a uniform 4Te-2D coating yielded an exceptional 23.7% PCE, along with excellent stability under heating and in an ambient environment.

The development of 2D perovskites incorporating conjugated ligands in PSCs is still in the initial stage. Although the rigidity of conjugated ligands has exhibited significant suppression of ion migration under heat stimulus and inhibition of moisture penetration through ligands, the stability of solar cell devices under operational conditions has not yet revealed outstanding performance that can compete with that of existing commercial solar panels. As such, the stability of the OSiPs under electric bias and light illumination requires further investigation. In addition, most of the 2D perovskite structures with conjugated ligands possess distorted inorganic octahedra, which may be arguably a potential problem for solar cell devices. Therefore, the design and implementation of conjugated ligands that create minimal lattice distortion will be the direction to pursue for ideal 2D perovskites in PSCs.

3.2. Application in LEDs. OSiPs have also attracted intensive attention in LED applications due to their outstanding optoelectronic properties and improved stability compared to their 3D counterparts. These distinctive attributes are expected to bring the performance of LED devices to the next level and eventually lead to their practical applications. Over the past few years, great progress has been made in the field of LEDs by employing alkyl-chain ligand (e.g., BA)-based quasi-2D perovskites as emitters. 143,144 Nevertheless, there is still a wide gap between quasi-2D perovskite LEDs and state-of-the-art LEDs, including organic and quantum dot LEDs, in terms of both the external quantum efficiency (EQE) and stability. The major hurdle behind the gap is that the alkyl-chain ligands in perovskite LEDs are typically insulating and soft, which could potentially prevent charge injection and limit the stability of the inorganic perovskite lattice. However, it becomes promising to tackle this challenge if the soft alkyl-chain ligands are substituted by bulky conjugated ligands to form OSiPs. This may benefit the charge injection, owing to the semiconducting nature of the conjugated ligands, and enhance the intrinsic stability due to the augmented rigidity of the perovskite lattice. The simplest conjugated ligand, PEA, has been intensively investigated to fabricate quasi-2D OSiP LEDs, yet with limited success in

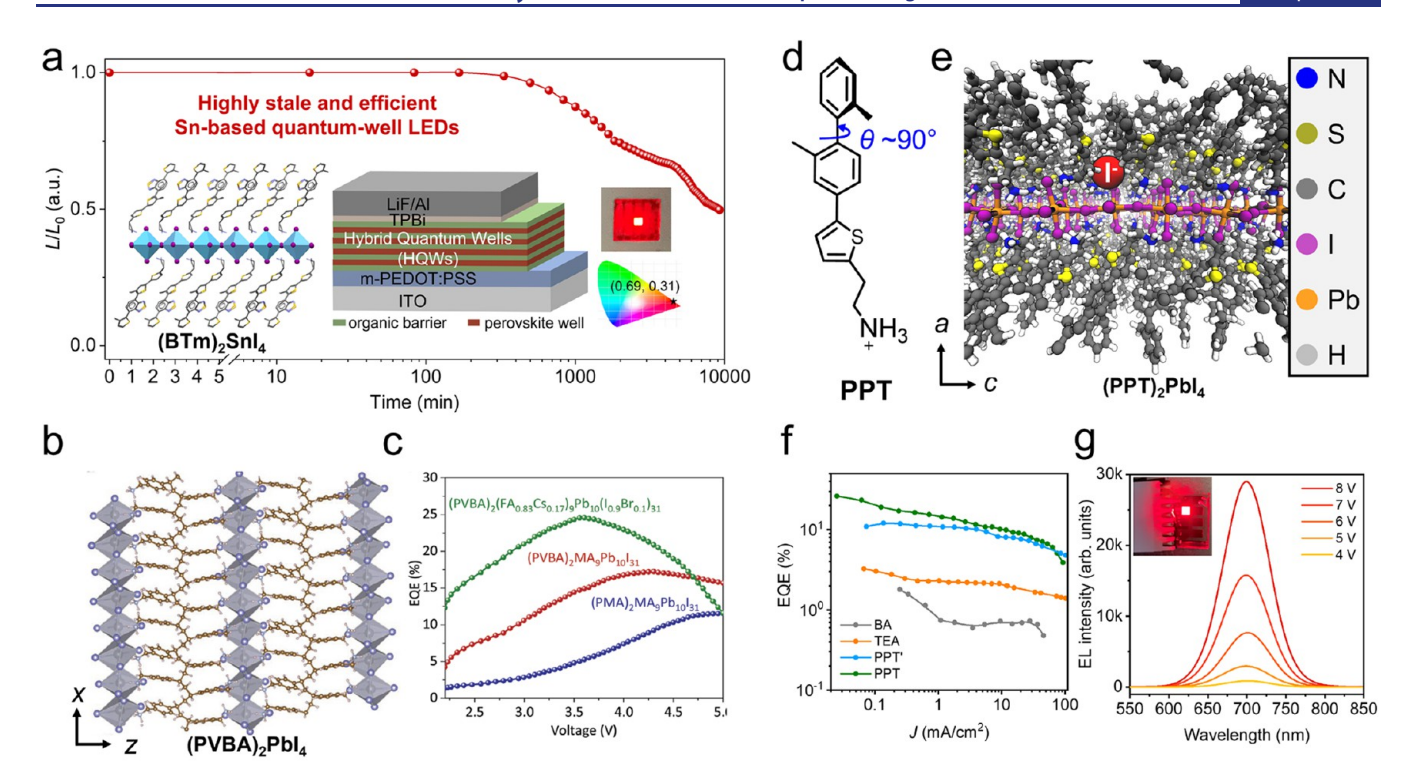


Figure 11. OSiP-based LEDs. (a) Stability of the LED device based on OSiP hybrid quantum wells. Insets (from left to right): single-crystal structure of (BTm)₂SnI₄; the configuration of the LED device; an image of a working device; chromaticity coordinates of the electroluminescence emission from OSiP LEDs. Reproduced with permission from ref 38. Copyright 2021 American Chemical Society. (b) Single-crystal structure of (PVBA)₂PbI₄ OSiP. (c) EQE of LED devices made from different ligands. Reproduced with permission from ref 71. Copyright 2021 John Wiley and Sons. (d) Molecular structure of PPT with a dihedral angle of 90° between two phenyl rings. (e) Molecular dynamics simulation of anion migration in (PPT)₂PbI₄. (f) EQE versus current density curves of OSiP LEDs based on different ligands (TEA is thiopheneethylammonium). (g) Electroluminescence spectra of a PPT-based LED under different driving voltages; the inset is an image of a working device. Reproduced with permission under a Creative Commons CC-BY license from ref 42. Copyright 2023 The Authors, published by Springer Nature.

promoting the device performance to a commercialization level because of its relatively wide band gap and insufficient bulkiness. $^{141,145-149}$

Initial attempts using much bulkier ligands were based on 1naphthylmethylammonium iodide (NMA, 2-6), which can facilitate the formation of self-organized multiple quantum wells with cascade energy transfer, resulting in a peak EQE of 11.7%. 140 Later on, Liang et al. designed and synthesized a series of novel molecular passivators, e.g., phenylimidazolium iodide, to passivate defects by forming low-dimensional perovskite phases on the 3D perovskite surface, demonstrating perovskite LED devices with improved thin-film quality and 15.6% EQE.³⁶ To further shrink the band gap of organic ligands and expand this idea to devices, Wang et al. developed a new Sn-based 2D perovskite LED device incorporating a semiconducting ligand, BTm (4-3), which has a molecular band gap very close to that of inorganic [SnI₆]⁴⁻ perovskite This molecular engineering approach results in strongly confined 2D organic-inorganic hybrid quantum wells (HQWs, inset in Figure 11a) with type I alignment featuring an improved charge transport property and enhanced stability (Figure 11a).

Utilizing femtosecond transient absorption spectroscopy, the energy transfer from semiconducting ligands to the perovskite lattice was observed to be faster than the intramolecular charge transfer in the organic layer. The faster energy transfer suggests that there is no additional energy loss in organic semiconducting ligands during carrier injection into the inorganic lattices. On this basis, red Sn-based OSiP LEDs were

demonstrated with high color purity and a peak EQE of 3.33%. Importantly, the LEDs showed exceptional operational stability of about 10⁴ min (>150 h) lifetime at an initial luminance of 40 cd m⁻², which made them the most stable Snbased OSiP LEDs reported at that time. In 2021, Chen et al. reported a polymer ligand (O-5, PVBA)-based OSiP ((PVBA)₂PbI₄, Figure 11b) with enhanced intrinsic stability, flexibility, and lattice rigidity.⁷¹ These characteristics enabled a reduced nonradiative recombination rate because of suppressed electron-phonon coupling and enhanced carrier mobility due to suppressed phonon scattering in OSiP films. By incorporating this OSiP into a typical p-i-n LED architecture, they achieved a maximum EQE of 23.2% and enhanced operation stability with optimal quantum well thickness and compositions (Figure 11c). This work represents a new strategy to improve the intrinsic stability and optoelectronic properties of OSiPs. Recently, Wang et al. innovatively designed and synthesized a novel bulky organic ligand, PPT (3-4, Figure 11d), in which a 90° dihedral angle resulting from two methyl group substituents can lead to the occupation of more free space between ligands. 42 Concomitantly, ion migration across the organic ligand layer was largely inhibited based on MD simulations (Figure 11e). Benefiting from the suppressed ion migration, the authors were able to control the n-phase within a much narrower range, resulting in dramatically improved optoelectronic properties of the quasi-2D OSiP thin films. Using femtosecond transient absorption spectroscopy, they demonstrated much faster energy-transfer dynamics than general cases with broad-phase distribution,

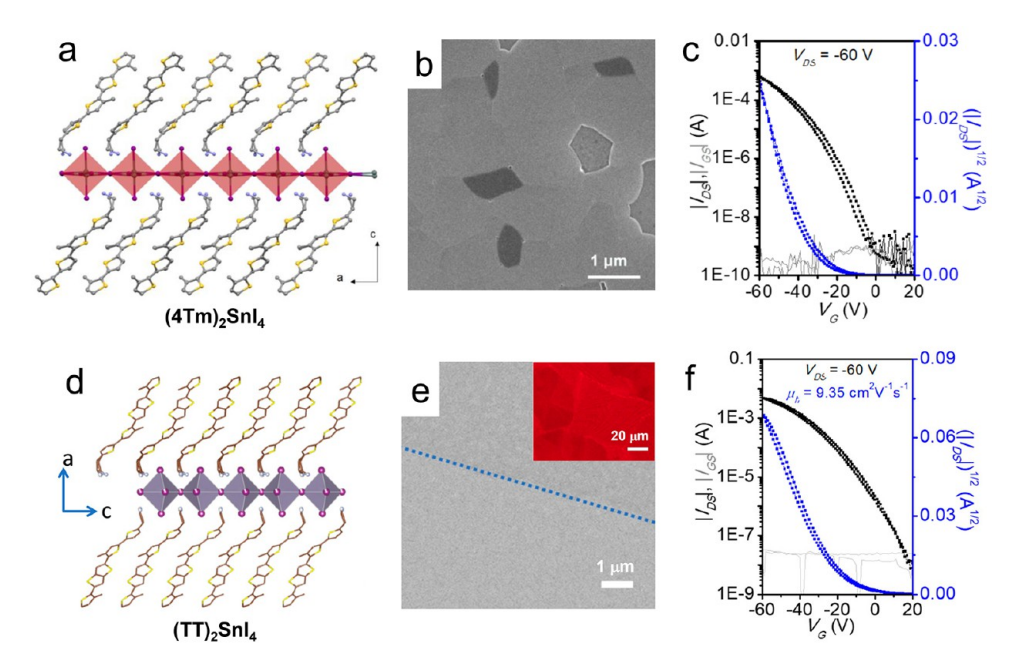


Figure 12. OSiP-based FETs. (a) Single-crystal structure of $(4\text{Tm})_2\text{SnI}_4$ OSiP. (b) SEM image of a 4Tm-based OSiP film. (c) Transfer characteristics of BG/TC FET devices based on $(4\text{Tm})_2\text{SnI}_4$ OSiPs. Reproduced with permission from ref 34. Copyright 2019 American Chemical Society. (d) Single-crystal structure of $(TT)_2\text{SnI}_4$ OSiP. (e) SEM image of a TT-based OSiP film; inset is the PL image. (f) Transfer characteristics of BG/TC FET devices based on $(TT)_2\text{SnI}_4$ OSiPs. Reproduced with permission from ref 40. Copyright 2021 American Chemical Society.

proven to be advantageous in reducing defect-related non-radiative recombination. As a result, the as-fabricated highly efficient deep-red LED devices revealed a peak EQE of 26.3% (Figure 11f) and extraordinary wavelength stability (Figure 11g) and tunability. Through judicious molecular design, OSiP-based LED devices hold great potential in further boosting the performance via addressing challenges related with the defect passivation and balance of the electron/hole injection.

3.3. Application in FETs. OSiPs are also emerging candidates for FET applications due to their enhanced charge transport capability originating from organic semiconducting ligands. 150 Meanwhile, the parallel growth orientation of OSiPs on substrates enables them to work effectively in such lateralstructured device configurations. As a benchmark material, PEA-ligand-based (PEA)₂SnI₄ can be made into a very smooth film, which exhibits a hole mobility of 0.15 cm² V⁻¹ s⁻¹ but with relatively poor device stability. 3,34,151-153 In sharp contrast, Gao et al. replaced PEA with a narrow-band-gap quaterthiophene-based organic ligand, 4Tm (4-2), to obtain a new type of OSiP ((4Tm)₂SnI₄, Figure 12a) with significantly strengthened ambient and thermal stability.³⁴ The enhanced charge transport of the 4Tm ligand and increased grain size in the OSiP film (Figure 12b) resulted in FET devices with reduced hysteresis and near 10-fold enhancement in hole mobility (2.32 cm² V⁻¹ s⁻¹, Figure 12c). By further extending the conjugation length of the organic ligand into the thienothiophene-based TT (4-11) ligand, Liang et al. reported Sn-based 2D perovskite thin films with larger grain texture (\sim 50 μ m, Figure 12d,e). 40 The mechanism of grain growth has not been fully elucidated yet, but it was suggested that the stronger intermolecular interactions from fused thiophene rings are considered the major factor in controlling the nucleation and crystallization, leading to highly ordered crystalline structures and extremely large grain sizes in OSiP thin films. Consequently, the authors demonstrated highperformance FETs with hole mobility up to 9.35 cm² V⁻¹ s⁻¹ (Figure 12f), ON/OFF current ratios higher than 10⁵, and excellent stability and reproducibility. Though the development of perovskite FETs is lagging behind the surge of perovskite photovoltaics, the use of OSiPs opens up a new direction that offers possibilities in modulating ion diffusion, defects, charge mobility, hysteresis, and stability of FETs via molecular engineering and mesoscopic crystallization control.

4. OUTLOOK

In this Perspective, the concept, brief history, and recent developments of OSiPs have been discussed. We focused on the molecular design, crystal growth, and fundamental optical and electronic properties of this fascinating family of materials. Several key features, including energy landscape management, efficient charge transfer, superior conductivity, and enhanced stability, make OSiPs very promising for a variety of device applications, including but not limited to solar cells, LEDs, and FETs. Many of these aspects are still in their infancy, accompanied by both challenges and new opportunities. In this section, we discuss possible future directions of OSiPs, spanning rational ligand design, novel functionalities, and advancing device performance, as well as some reverse thinking—utilizing a perovskite lattice to template organic materials.

4.1. Rational Design and Synthesizability of 2D OSiPs. The limited exploration of ligand chemistries creates opportunities for innovation and a need for design rules to guide exploration. Most exploration has been focused on varying aromatic moieties and linker length, but other aspects of the ligands bear investigation. First, side chains on the aromatic bodies can modulate physical properties (e.g., solubility and hydrophobicity) that affect perovskite properties (e.g., environmental stability and ligand organization). In particular, functionalizing the non-ammonium terminal group can induce new interlayer interactions that compete with the

ammonium bonding interaction with the inorganic lattice. In addition, small structural variations in ligands may influence the overall structural distortion and affect the corresponding optoelectronic properties of OSiPs. Second, new ligand design may lead to novel crystal structures beyond the existing RP, DJ, and ACI phases or the ability to control 2D phases with intermediate *n*-numbers. For example, recent work has shown that ligand selection can modulate the distribution of layer numbers in RP-phase films, but the general design rules and limits of this influence remain unknown. 42 Third, it could be promising to modulate the control of crystal rigidity, ion diffusion, and electron-phonon coupling via molecular design. For instance, rigid fused-ring conjugated moieties may translate the molecular stiffness into the inorganic framework and further influence the polaron formation, charge transport, and light emission properties. Finally, these explorations would be greatly accelerated by computational modeling and machine-learning models that could focus precious synthetic efforts. Synthesizing a conjugated ligand is a demanding process that usually requires several steps and isolation procedures to obtain products with high purity. Besides the work of predicting 2D perovskites using ML models reported by Lyu et al. and Lin et al., 102,116 it is of interest to extend the current chemical scope with diverse structural combinations and scrutinize the structure-property relationships between ligands and the resulting 2D and quasi-2D perovskites.

4.2. OSiPs with Novel Functionalities. Currently, only type I and II band alignments have been realized at the organic-inorganic interface within the OSiP crystals. To implement spontaneous charge transfer and electrical doping, the type III-broken gap configuration is also desirable but has not yet been realized. In this regard, exotic ligands with extrastrong donor/acceptor moieties 154 may be designed for the construction of OSiPs with type III band configuration. Moreover, designing ligands with these characteristics provides opportunities to realize a type II alignment in high-n 2D perovskites. Doping of organic semiconductors is a wellestablished but still active area of research, and much can be learned from existing literature. 155-157 However, an important question is whether these doped molecules are stable enough and compatible with the normal perovskite crystal growth conditions, which involve a polar solvent, mild heating, and redox-active halide anions (also trace halide radicals). Synthesis of a cationic version of such extremely strong donor or acceptor molecules can be even more challenging.

Except for light and bias, mechanical stimuli may also be used to manipulate the properties to realize new perovskite functionalities. 2D OSiPs inherit the "soft" lattices from 3D perovskites, which give versatile structural response and "electronic compressibility". 158,159 Recently, Guo et al. applied pressure to OSiPs, allowing the reconfiguration of band edge state. 160 A key finding is that the HOMO-LUMO gaps of the organic semiconductor moieties are less "compressible" than the VBM-CBM gap of the inorganic sheet. In other words, the band gap shrinking of the inorganic layer with respect to the pressure is much faster than that of the organic layer. As a result, band alignment switching can be realized. For example, for (BTm)₂PbI₄, a clean transition of band alignment from reversed-type I to type II to type I was observed with increased pressure, revealing an ON/OFF optoelectronic response. Further directions can be focused on extending the scope of perovskite materials under pressure gating, directional pressure

to specific crystal facets, and even combining additional external stimuli such as bias or heat. 161

4.3. Achieving Higher Quality Thin Films and Better Device Performance. The applications of OSiPs in solar cells, LEDs, and FETs are at the beginning stages. The incorporation of OSiP into devices is expected to significantly alter the charge-transfer properties and lattice stability, which are critical to making new breakthroughs in device performance. However, there are still some remaining questions that need to be answered before bridging the gap between fundamental studies and device applications. First of all, the bulkiness and unique intermolecular interactions of conjugated ligands will result in different interactions with solvent and $[BX_6]^{4-}$ octahedra, in which they differ from the conventional ligands during the fast crystallization process of film formation. Therefore, extra efforts are needed to improve the quality of thin films, including the thickness, morphology, crystallinity, grain size, phase purity, and crystal orientation, through a deep understanding of the ligands' role in the crystallization process. Second, to retain the full potential of OSiPs in device stability, further investigation of the stability of OSiPs under operational conditions is required. The rigidity and bulkiness of conjugated ligands will suppress ion migration but will also introduce lattice strains, which may change the degradation mechanism under applied voltage, heat, and light. Thus, understanding and addressing these processes will facilitate the design of stable devices.

Besides these challenges, there are tremendous opportunities that the OSiP structures can offer to current devices. For devices with multiple layers, OSiPs can provide programmable tunability for interface energy level alignment. For example, achieving proper energy level alignment between the perovskite and electron-transporting layer (ETL) is challenging through conventional 2D/3D heterojunction. However, properly designed OSiPs with shallow LUMO ligands can form n-type semiconducting materials, which can address the energy alignment issue at the ETL/perovskite interface in either p-i-n or n-i-p devices. Moreover, through judicious ligand design, devices with OSiP materials can also enable tunable affinity with an electron/hole transporting layer, which are usually organic semiconductors. Therefore, the OSiP interface layer can act as a bridge between the organic and inorganic semiconductors via its bifunctional property. The conductivity of OSiPs has been discussed based on crystal structure and the packing geometry of organic molecular layers, which is correlated with the device performance. However, a fundamental understanding of electron delocalization and carrier dynamics will facilitate the future design of conjugated ligands for overcoming the conductivity barrier of 2D perovskites.

4.4. Inverse Templating—Using Perovskites to Control and Manipulate Organic Materials. At the current stage, organic materials are usually designed to fit into the perovskite lattices and impart their novel functionalities to the 2D perovskites, but the reverse, namely, using an inorganic perovskite lattice to control the behaviors of organic molecules, has been less explored. Specifically, the unique structure of 2D perovskite lattices could serve as a template to guide the selfassembly of organic materials, thus directing the construction of large-scale and high-quality crystalline organic films for optoelectronic applications. In addition, the inorganic lattice could act as a matrix to weaken the intermolecular interaction between organic molecules and help reduce or eliminate the

aggregation-induced quenching effect that has troubled the organic optoelectronics field for a long time. This strategy may further boost the device performance of OLEDs and organic lasers when considering improved photoluminescence quantum yield of organic emitters after their incorporation into the inorganic matrix. More importantly, organic emitters will generate singlet and triplet excitons with a 1:3 ratio under electrical excitation based on spin statistics. Triplet excitons are typically not emissive and can also cause extra exciton losses in devices via triplet absorption, triplet—triplet annihilation, triplet—singlet annihilation, etc. Thus, by rationally designing an inorganic perovskite lattice with suitable triplet energy levels, it can be expected to quench the triplets or reharvest the triplets in organic emitters for more efficient light-emitting devices.

The challenges and possible future directions discussed above are manifold, but they are still only based on a limited understanding of the design rules and performance limits of emerging OSiP materials and devices. We are confident that the field will grow more rapidly soon and many new opportunities will emerge. We hope that this Perspective will have a positive impact on the community and inspire new ideas and discussions in the near future.

AUTHOR INFORMATION

Corresponding Author

Letian Dou — Davidson School of Chemical Engineering, Purdue University, West Lafayette, Indiana 47907, United States; Department of Chemistry and Birck Nanotechnology Center, Purdue University, West Lafayette, Indiana 47907, United States; orcid.org/0000-0001-6411-8591; Email: dou10@purdue.edu

Authors

Jiaonan Sun − Davidson School of Chemical Engineering, Purdue University, West Lafayette, Indiana 47907, United States; ocid.org/0000-0002-4102-0564

Kang Wang — Davidson School of Chemical Engineering, Purdue University, West Lafayette, Indiana 47907, United States; [®] orcid.org/0000-0002-7178-1225

Ke Ma – Davidson School of Chemical Engineering, Purdue University, West Lafayette, Indiana 47907, United States

Jee Yung Park — Davidson School of Chemical Engineering, Purdue University, West Lafayette, Indiana 47907, United States; orcid.org/0000-0002-9814-6563

Zih-Yu Lin — Davidson School of Chemical Engineering, Purdue University, West Lafayette, Indiana 47907, United States

Brett M. Savoie — Davidson School of Chemical Engineering, Purdue University, West Lafayette, Indiana 47907, United States; orcid.org/0000-0002-7039-4039

Complete contact information is available at: https://pubs.acs.org/10.1021/jacs.3c02143

Notes

The views expressed herein do not necessarily represent the views of the U.S. Department of Energy or the United States Government.

The authors declare no competing financial interest.

ACKNOWLEDGMENTS

The authors acknowledge funding support from the U.S. Department of Energy's Office of Energy Efficiency and

Renewable Energy (EERE) under the Solar Energy Technologies Office Award DE-EE0009519. J.Y.P. acknowledges support from the National Science Foundation under Award No. 2110706-DMR. K.M. acknowledges financial support from Lillian Gilbreth Postdoctoral Fellowships. We thank Lukas Yi Peng and Aline Carla Kruger for proofreading the manuscript.

REFERENCES

- (1) Watthage, S. C.; Song, Z.; Phillips, A. B.; Heben, M. J. *Evolution of Perovskite Solar Cells*; Elsevier Inc., 2018. DOI: 10.1016/B978-0-12-812915-9.00003-4.
- (2) Song, Z.; Watthage, S. C.; Phillips, A. B.; Heben, M. J. Pathways toward High-Performance Perovskite Solar Cells: Review of Recent Advances in Organo-Metal Halide Perovskites for Photovoltaic Applications. *J. Photonics Energy* **2016**, *6* (2), 022001.
- (3) Kagan, C. R.; Mitzi, D. B.; Dimitrakopoulos, C. D. Organic-Inorganic Hybrid Materials as Semiconducting Channels in Thin-Film Field-Effect Transistors. *Science* **1999**, 286 (5441), 945–947.
- (4) Kojima, A.; Teshima, K.; Shirai, Y.; Miyasaka, T. Organometal Halide Perovskites as Visible-Light Sensitizers for Photovoltaic Cells. *J. Am. Chem. Soc.* **2009**, *131* (17), 6050–6051.
- (5) Xing, G.; Mathews, N.; Sun, S.; Lim, S. S.; Lam, Y. M.; Gratzel, M.; Mhaisalkar, S.; Sum, T. C. Long-Range Balanced Electron- and Hole-Transport Lengths in Organic-Inorganic CH₃NH₃PbI₃. *Science* **2013**, 342 (6156), 344–347.
- (6) Min, H.; Lee, D. Y.; Kim, J.; Kim, G.; Lee, K. S.; Kim, J.; Paik, M. J.; Kim, Y. K.; Kim, K. S.; Kim, M. G.; Shin, T. J.; Il Seok, S. Perovskite Solar Cells with Atomically Coherent Interlayers on SnO₂ Electrodes. *Nature* **2021**, *598* (7881), 444–450.
- (7) Zhou, H.; Chen, Q.; Li, G.; Luo, S.; Song, T. B.; Duan, H. S.; Hong, Z.; You, J.; Liu, Y.; Yang, Y. Interface Engineering of Highly Efficient Perovskite Solar Cells. *Science* **2014**, *345* (6196), 542–546.
- (8) Arora, N.; Dar, M. I.; Hinderhofer, A.; Pellet, N.; Schreiber, F.; Zakeeruddin, S. M.; Grätzel, M. Perovskite Solar Cells with CuSCN Hole Extraction Layers Yield Stabilized Efficiencies Greater than 20%. *Science* **2017**, 358 (6364), 768–771.
- (9) Numata, Y.; Sanehira, Y.; Ishikawa, R.; Shirai, H.; Miyasaka, T. Thiocyanate Containing Two-Dimensional Cesium Lead Iodide Perovskite, Cs₂PbI₂(SCN)₂: Characterization, Photovoltaic Application, and Degradation Mechanism. *ACS Appl. Mater. Interfaces* **2018**, 10 (49), 42363–42371.
- (10) Li, J.; Yu, Q.; He, Y.; Stoumpos, C. C.; Niu, G.; Trimarchi, G. G.; Guo, H.; Dong, G.; Wang, D.; Wang, L.; Kanatzidis, M. G. Cs₂PbI₂Cl₂, All-Inorganic Two-Dimensional Ruddlesden-Popper Mixed Halide Perovskite with Optoelectronic Response. *J. Am. Chem. Soc.* **2018**, *140* (35), 11085–11090.
- (11) Zhao, X.; Liu, T.; Burlingame, Q. C.; Liu, T.; Holley, R.; Cheng, G.; Yao, N.; Gao, F.; Loo, Y.-L. Accelerated Aging of All-Inorganic, Interface-Stabilized Perovskite Solar Cells. *Science* **2022**, 377, 307–310.
- (12) Li, X.; Hoffman, J. M.; Kanatzidis, M. G. The 2D Halide Perovskite Rulebook: How the Spacer Influences Everything from the Structure to Optoelectronic Device Efficiency. *Chem. Rev.* **2021**, *121* (4), 2230–2291.
- (13) Mao, L.; Ke, W.; Pedesseau, L.; Wu, Y.; Katan, C.; Even, J.; Wasielewski, M. R.; Stoumpos, C. C.; Kanatzidis, M. G. Hybrid Dion-Jacobson 2D Lead Iodide Perovskites. *J. Am. Chem. Soc.* **2018**, *140* (10), 3775–3783.
- (14) Soe, C. M. M.; Stoumpos, C. C.; Kepenekian, M.; Traoré, B.; Tsai, H.; Nie, W.; Wang, B.; Katan, C.; Seshadri, R.; Mohite, A. D.; Even, J.; Marks, T. J.; Kanatzidis, M. G. New Type of 2D Perovskites with Alternating Cations in the Interlayer Space, (C(NH₂)₃)-(CH₃NH₃)NPb_nI3_{n+1}: Structure, Properties, and Photovoltaic Performance. *J. Am. Chem. Soc.* **2017**, *139* (45), 16297–16309.
- (15) Straus, D. B.; Kagan, C. R. Electrons, Excitons, and Phonons in Two-Dimensional Hybrid Perovskites: Connecting Structural, Optical, and Electronic Properties. *J. Phys. Chem. Lett.* **2018**, 9 (6), 1434–1447.

- (16) Dunlap-Shohl, W. A.; Barraza, E. T.; Barrette, A.; Dovletgeldi, S.; Findik, G.; Dirkes, D. J.; Liu, C.; Jana, M. K.; Blum, V.; You, W.; Gundogdu, K.; Stiff-Roberts, A. D.; Mitzi, D. B. Tunable Internal Quantum Well Alignment in Rationally Designed Oligomer-Based Perovskite Films Deposited by Resonant Infrared Matrix-Assisted Pulsed Laser Evaporation. *Mater. Horizons* 2019, 6 (8), 1707–1716. (17) Liu, C.; Huhn, W.; Du, K. Z.; Vazquez-Mayagoitia, A.; Dirkes, D.; You, W.; Kanai, Y.; Mitzi, D. B.; Blum, V. Tunable Semiconductors: Control over Carrier States and Excitations in Layered Hybrid Organic-Inorganic Perovskites. *Phys. Rev. Lett.* 2018, 121 (14),
- (18) Mitzi, D. B.; Chondroudis, K.; Kagan, C. R. Design, Structure, and Optical Properties of Organic-Inorganic Perovskites Containing an Oligothiophene Chromophore. *Inorg. Chem.* **1999**, 38 (26), 6246–6256.
- (19) Braun, M.; Tuffentsammer, W.; Wachtel, H.; Wolf, H. C. Pyrene as Emitting Chromophore in Organic-Inorganic Lead Halide-Based Layered Perovskites with Different Halides. *Chem. Phys. Lett.* **1999**, 307 (5–6), 373–378.
- (20) Takeoka, Y.; Asai, K.; Rikukawa, M.; Sanui, K. Incorporation of Conjugated Polydiacetylene Systems into Organic-Inorganic Quantum-Well Structures. *Chem. Commun.* **2001**, 2592–2593.
- (21) Ema, K.; Inomata, M.; Kato, Y.; Kunugita, H.; Era, M. Nearly Perfect Triplet-Triplet Energy Transfer from Wannier Excitons to Naphthalene in Organic-Inorganic Hybrid Quantum-Well Materials. *Phys. Rev. Lett.* **2008**, *100* (25), 257401.
- (22) Era, M.; Kobayashi, T.; Sakaguchi, K.; Tsukamoto, E.; Oishi, Y. Electric Conduction of PbBr-Based Layered Perovskite Organic-Inorganic Superlattice Having Carbazole Chromophore-Linked Ammonium Molecule as an Organic Layer. *Org. Electron.* **2013**, *14* (5), 1313–1317.
- (23) Cortecchia, D.; Soci, C.; Cametti, M.; Petrozza, A.; Martí-Rujas, J. Crystal Engineering of a Two-Dimensional Lead-Free Perovskite with Functional Organic Cations by Second-Sphere Coordination. *ChemPlusChem.* **2017**, 82 (5), 681–685.
- (24) Du, K. Z.; Tu, Q.; Zhang, X.; Han, Q.; Liu, J.; Zauscher, S.; Mitzi, D. B. Two-Dimensional Lead(II) Halide-Based Hybrid Perovskites Templated by Acene Alkylamines: Crystal Structures, Optical Properties, and Piezoelectricity. *Inorg. Chem.* **2017**, *56* (15), 9291–9302.
- (25) Papavassiliou, G. C.; Mousdis, G. A.; Pagona, G.; Karousis, N.; Vidali, M. S. Room Temperature Enhanced Blue-Green, Yellow-Orange and Red Phosphorescence from Some Compounds of the Type $(CH_3NH_3)_{n-1}(1-Naphthylmethyl Ammonium)_2Pb_n(Cl_xBr_{1-x})-3_{n+1}$ (with N=1, 2 and $0 \le x \le 1$) and Related Observations from Similar Compounds. *J. Lumin.* **2014**, *149*, 287–291.
- (26) Chondroudis, K.; Mitzi, D. B. Electroluminescence from an Organic-Inorganic Perovskite Incorporating a Quaterthiophene Dye within Lead Halide Perovskite Layers. *Chem. Mater.* **1999**, *11* (11), 3028–3030.
- (27) Gao, Y.; Dou, L. Organic Semiconductor-Incorporated Two-Dimensional Halide Perovskites. *Natl. Sci. Rev.* **2022**, 9 (5), 2021–2023.
- (28) Gao, Y.; Shi, E.; Deng, S.; Shiring, S. B.; Snaider, J. M.; Liang, C.; Yuan, B.; Song, R.; Janke, S. M.; Liebman-Peláez, A.; Yoo, P.; Zeller, M.; Boudouris, B. W.; Liao, P.; Zhu, C.; Blum, V.; Yu, Y.; Savoie, B. M.; Huang, L.; Dou, L. Molecular Engineering of Organic-Inorganic Hybrid Perovskites Quantum Wells. *Nat. Chem.* **2019**, *11* (12), 1151–1157.
- (29) Gao, Y.; Wei, Z.; Hsu, S. N.; Boudouris, B. W.; Dou, L. Two-Dimensional Halide Perovskites Featuring Semiconducting Organic Building Blocks. *Mater. Chem. Front.* **2020**, *4* (12), 3400–3418.
- (30) Liang, A.; Ma, K.; Gao, Y.; Dou, L. Tailoring Anchoring Groups in Low-Dimensional Organic Semiconductor-Incorporated Perovskites. *Small Struct.* **2022**, 3 (3), 2100173.
- (31) Wang, K.; Park, J. Y.; Akriti; Dou, L. Two-dimensional Halide Perovskite Quantum-well Emitters: A Critical Review. *EcoMat* **2021**, 3 (3), No. e12104.

- (32) Zhao, W.; Hsu, S. N.; Boudouris, B. W.; Dou, L. Two-Dimensional Organic Semiconductor-Incorporated Perovskite (OSiP) Electronics. ACS Appl. Electron. Mater. 2021, 3 (12), 5155–5164.
- (33) Wei, Z.; Wang, K.; Zhao, W.; Gao, Y.; Hu, Q.; Chen, K.; Dou, L. A Selenophene-Containing Conjugated Organic Ligand for Two-Dimensional Halide Perovskites. *Chem. Commun.* **2021**, *57* (87), 11469–11472.
- (34) Gao, Y.; Wei, Z.; Yoo, P.; Shi, E.; Zeller, M.; Zhu, C.; Liao, P.; Dou, L. Highly Stable Lead-Free Perovskite Field-Effect Transistors Incorporating Linear Π-Conjugated Organic Ligands. *J. Am. Chem. Soc.* **2019**, *141* (39), 15577–15585.
- (35) Coffey, A. H.; Yang, S. J.; Gómez, M.; Finkenauer, B. P.; Terlier, T.; Zhu, C.; Dou, L. Controlling Crystallization of Quasi-2D Perovskite Solar Cells: Incorporating Bulky Conjugated Ligands. *Adv. Energy Mater.* **2022**, 2201501.
- (36) Liang, A.; Wang, K.; Gao, Y.; Finkenauer, B. P.; Zhu, C.; Jin, L.; Huang, L.; Dou, L. Highly Efficient Halide Perovskite Light-Emitting Diodes via Molecular Passivation. *Angew. Chem., Int. Ed.* **2021**, *60* (15), 8337–8343.
- (37) Hsu, S. N.; Zhao, W.; Gao, Y.; Akriti; Segovia, M.; Xu, X.; Boudouris, B. W.; Dou, L. Thermoelectric Performance of Lead-Free Two-Dimensional Halide Perovskites Featuring Conjugated Ligands. *Nano Lett.* **2021**, 21 (18), 7839–7844.
- (38) Wang, K.; Jin, L.; Gao, Y.; Liang, A.; Finkenauer, B. P.; Zhao, W.; Wei, Z.; Zhu, C.; Guo, T. F.; Huang, L.; Dou, L. Lead-Free Organic-Perovskite Hybrid Quantum Wells for Highly Stable Light-Emitting Diodes. ACS Nano 2021, 15 (4), 6316–6325.
- (39) Ma, K.; Hsu, S.-N.; Gao, Y.; Wei, Z.; Jin, L.; Finkenauer, B. P.; Huang, L.; Boudouris, B. W.; Mei, J.; Dou, L. Organic Cation Engineering for Vertical Charge Transport in Lead-Free Perovskite Quantum Wells. *Small Sci.* **2021**, *1* (8), 2000024.
- (40) Liang, A.; Gao, Y.; Asadpour, R.; Wei, Z.; Finkenauer, B. P.; Jin, L.; Yang, J.; Wang, K.; Chen, K.; Liao, P.; Zhu, C.; Huang, L.; Boudouris, B. W.; Alam, M. A.; Dou, L. Ligand-Driven Grain Engineering of High Mobility Two-Dimensional Perovskite Thin-Film Transistors. *J. Am. Chem. Soc.* **2021**, *143* (37), 15215–15223.
- (41) Ma, K.; Atapattu, H. R.; Zhao, Q.; Gao, Y.; Finkenauer, B. P.; Wang, K.; Chen, K.; Park, S. M.; Coffey, A. H.; Zhu, C.; Huang, L.; Graham, K. R.; Mei, J.; Dou, L. Multifunctional Conjugated Ligand Engineering for Stable and Efficient Perovskite Solar Cells. *Adv. Mater.* **2021**, 33 (32), 2100791.
- (42) Wang, K.; Lin, Z. Y.; Zhang, Z.; Jin, L.; Ma, K.; Coffey, A. H.; Atapattu, H. R.; Gao, Y.; Park, J. Y.; Wei, Z.; Finkenauer, B. P.; Zhu, C.; Meng, X.; Chowdhury, S. N.; Chen, Z.; Terlier, T.; Do, T. H.; Yao, Y.; Graham, K. R.; Boltasseva, A.; Guo, T. F.; Huang, L.; Gao, H.; Savoie, B. M.; Dou, L. Suppressing Phase Disproportionation in Quasi-2D Perovskite Light-Emitting Diodes. *Nat. Commun.* 2023, 14 (1), 397.
- (43) Zhang, F.; Lu, H.; Tong, J.; Berry, J. J.; Beard, M. C.; Zhu, K. Advances in Two-Dimensional Organic-Inorganic Hybrid Perovskites. *Energy Environ. Sci.* **2020**, *13* (4), 1154–1186.
- (44) Zhao, X.; Liu, T.; Loo, Y. L. Advancing 2D Perovskites for Efficient and Stable Solar Cells: Challenges and Opportunities. *Adv. Mater.* **2022**, *34* (3), 2105849.
- (45) Mao, L.; Stoumpos, C. C.; Kanatzidis, M. G. Two-Dimensional Hybrid Halide Perovskites: Principles and Promises. *J. Am. Chem. Soc.* **2019**, *141* (3), 1171–1190.
- (46) Zhu, X. H.; Mercier, N.; Frère, P.; Blanchard, P.; Roncali, J.; Allain, M.; Pasquier, C.; Riou, A. Effect of Mono- versus Di-Ammonium Cation of 2,2'-Bithiophene Derivatives on the Structure of Organic-Inorganic Hybrid Materials Based on Iodo Metallates. *Inorg. Chem.* **2003**, 42 (17), 5330–5339.
- (47) Dong, Y.; Dong, X.; Lu, D.; Chen, M.; Zheng, N.; Wang, R.; Li, Q.; Xie, Z.; Liu, Y. Orbital Interactions between Organic Semiconductor Spacer and Inorganic Layer in Dion-Jacobson Perovskite Enable Efficient Solar Cells. *Adv. Mater.* **2023**, *35* (3), 2205258.
- (48) Hu, H.; Meier, F.; Zhao, D.; Abe, Y.; Gao, Y.; Chen, B.; Salim, T.; Chia, E. E. M.; Qiao, X.; Deibel, C.; Lam, Y. M. Efficient Room-Temperature Phosphorescence from Organic-Inorganic Hybrid Per-

- ovskites by Molecular Engineering. Adv. Mater. 2018, 30 (36), 1707621.
- (49) Era, M.; Maeda, K.; Tsutsui, T. Enhanced Phosphorescence from Naphthalene-Chromophore Incorporated into Lead Bromide-Based Layered Perovskite Having Organic-Inorganic Superlattice Structure. *Chem. Phys. Lett.* **1998**, 296 (3–4), 417–420.
- (50) Xu, Z.; Lu, D.; Liu, F.; Lai, H.; Wan, X.; Zhang, X.; Liu, Y.; Chen, Y. Phase Distribution and Carrier Dynamics in Multiple-Ring Aromatic Spacer-Based Two-Dimensional Ruddlesden-Popper Perovskite Solar Cells. ACS Nano 2020, 14 (4), 4871–4881.
- (51) Passarelli, J. V.; Fairfield, D. J.; Sather, N. A.; Hendricks, M. P.; Sai, H.; Stern, C. L.; Stupp, S. I. Enhanced Out-of-Plane Conductivity and Photovoltaic Performance in n = 1 Layered Perovskites through Organic Cation Design. *J. Am. Chem. Soc.* **2018**, *140* (23), 7313–7323
- (52) Hu, H.; Zhao, D.; Gao, Y.; Qiao, X.; Salim, T.; Chen, B.; Chia, E. E. M.; Grimsdale, A. C.; Lam, Y. M. Harvesting Triplet Excitons in Lead-Halide Perovskites for Roomerature Phosphorescence. *Chem. Mater.* **2019**, *31* (7), 2597–2602.
- (53) Zhao, R.; Sabatini, R. P.; Zhu, T.; Wang, S.; Morteza Najjarian, A.; Johnston, A.; Lough, A. J.; Hoogland, S.; Sargent, E. H.; Seferos, D. S. Rigid Conjugated Diamine Templates for Stable Dion-Jacobson-Type Two-Dimensional Perovskites. *J. Am. Chem. Soc.* **2021**, *143* (47), 19901–19908.
- (54) Park, I. H.; Chu, L.; Leng, K.; Choy, Y. F.; Liu, W.; Abdelwahab, I.; Zhu, Z.; Ma, Z.; Chen, W.; Xu, Q. H.; Eda, G.; Loh, K. P. Highly Stable Two-Dimensional Tin(II) Iodide Hybrid Organic-Inorganic Perovskite Based on Stilbene Derivative. *Adv. Funct. Mater.* **2019**, 29 (39), 1904810.
- (55) Sasai, R.; Shinomura, H. Preparation and Optical Characteristics of Layered Perovskite-Type Lead-Bromide-Incorporated Azobenzene Chromophores. *J. Solid State Chem.* **2013**, *198*, 452–458.
- (56) Fillafer, N.; Seewald, T.; Schmidt-Mende, L.; Polarz, S. Interfacial Charge Transfer Processes in 2D and 3D Semiconducting Hybrid Perovskites: Azobenzene as Photoswitchable Ligand. *Beilstein J. of Nanotechnol.* **2020**, *11* (1), 466–479.
- (57) Jemli, K.; Audebert, P.; Galmiche, L.; Trippé-Allard, G.; Garrot, D.; Lauret, J. S.; Deleporte, E. Two-Dimensional Perovskite Activation with an Organic Luminophore. *ACS Appl. Mater. Interfaces* **2015**, *7* (39), 21763–21769.
- (58) Yang, S.; Wu, D.; Gong, W.; Huang, Q.; Zhen, H.; Ling, Q.; Lin, Z. Highly Efficient Room-Temperature Phosphorescence and Afterglow Luminescence from Common Organic Fluorophores in 2D Hybrid Perovskites. *Chem. Sci.* **2018**, *9* (48), 8975–8981.
- (59) Sun, J.; Ma, K.; Lin, Z.-Y.; Tang, Y.; Varadharajan, D.; Chen, A. X.; Atapattu, H. R.; Lee, Y. H.; Chen, K.; Boudouris, B. W.; Graham, K. R.; Lipomi, D. J.; Mei, J.; Savoie, B. M.; Dou, L. Tailoring Molecular-Scale Contact at Perovskite/Polymeric Hole Transporting Material Interface for Efficient Solar Cells. *Adv. Mater.* **2023**, *35*, 2300647.
- (60) Ma, K.; Sun, J.; Atapattu, R. H.; Larson, W. B.; Yang, H.; Sun, D.; Chen, K.; Wang, K.; Lee, Y.; Tang, Y.; Bhoopalam, A.; Huang, L.; Graham, R. K.; Mei, J.; Dou, L. Holistic Energy Landscape Management in 2D/3D Heterojunction via Molecular Engineering for Efficient Perovskite Solar Cells. *Sci. Adv.* **2023**, 9 (23), No. eadg0032.
- (61) Xue, J.; Wang, R.; Chen, X.; Yao, C.; Jin, X.; Wang, K. L.; Huang, W.; Huang, T.; Zhao, Y.; Zhai, Y.; Meng, D.; Tan, S.; Liu, R.; Wang, Z. K.; Zhu, C.; Zhu, K.; Beard, M. C.; Yan, Y.; Yang, Y. Reconfiguring the Band-Edge States of Photovoltaic Perovskites by Conjugated Organic Cations. *Science* **2021**, 371 (6529), 636–640.
- (62) Van Gompel, W. T. M.; Herckens, R.; Denis, P. H.; Mertens, M.; Gélvez-Rueda, M. C.; Van Hecke, K.; Ruttens, B.; D'Haen, J.; Grozema, F. C.; Lutsen, L.; Vanderzande, D. 2D Layered Perovskite Containing Functionalised Benzothieno-Benzothiophene Molecules: Formation, Degradation, Optical Properties and Photoconductivity. J. Mater. Chem. C 2020, 8 (21), 7181–7188.
- (63) Mishra, A.; Ahlawat, P.; Fish, G. C.; Jahanbakhshi, F.; Mladenović, M.; Almalki, M.; Ruiz-Preciado, M. A.; Gelvéz-Rueda,

- M. C.; Kubicki, D. J.; Schouwink, P. A.; Dufoulon, V.; Schneeberger, T.; Aslanzadeh, A.; Grozema, F. C.; Zakeeruddin, S. M.; Moser, J. E.; Rothlisberger, U.; Emsley, L.; Milić, J. v.; Grätzel, M. Naphthalenediimide/Formamidinium-Based Low-Dimensional Perovskites. *Chem. Mater.* **2021**, 33 (16), 6412–6420.
- (64) Li, X.; Yang, J.; Song, Z.; Chen, R.; Ma, L.; Li, H.; Jia, J.; Meng, J.; Li, X.; Yi, M.; Sun, X. Naphthalene Diimide Ammonium Directed Single-Crystalline Perovskites with "Atypical" Ambipolar Charge Transport Signatures in Two-Dimensional Limit. *ACS Appl. Energy Mater.* **2018**, *1* (9), 4467–4472.
- (65) Wang, Y.; Yan, D.; Wang, L.; Wang, D.; Tang, B. Z. Aggregation-Induced Emission Luminogens Sensitized Quasi-2D Hybrid Perovskites with Unique Photoluminescence and High Stability for Fabricating White Light-Emitting Diodes. *Adv. Sci.* **2021**, *8* (15), 2100811.
- (66) Liu, C.; Fang, Z.; Sun, J.; Shang, M.; Zheng, K.; Yang, W.; Ge, Z. Donor-Acceptor-Donor Type Organic Spacer for Regulating the Quantum Wells of Dion-Jacobson 2D Perovskites. *Nano Energy* **2022**, 93, 106800.
- (67) Lédée, F.; Audebert, P.; Trippé-Allard, G.; Galmiche, L.; Garrot, D.; Marrot, J.; Lauret, J. S.; Deleporte, E.; Katan, C.; Even, J.; Quarti, C. Tetrazine Molecules as an Efficient Electronic Diversion Channel in 2D Organic-Inorganic Perovskites. *Mater. Horiz.* **2021**, 8 (5), 1547–1560.
- (68) Isikgor, F. H.; Reddy, C. D.; Li, M.; Coskun, H.; Li, B.; Zhang, Y. W.; Pennycook, S. J.; Ouyang, J. Self-Assembled Atomically Thin Hybrid Conjugated Polymer Perovskites with Two-Dimensional Structure. J. Mater. Chem. C 2018, 6 (31), 8405–8410.
- (69) Era, M.; Yoneda, S.; Sano, T.; Noto, M. Preparation of Amphiphilic Poly(Thiophene)s and Their Application for the Construction of Organic-Inorganic Superlattices. *Thin Solid Films* **2003**, 438, 322–325.
- (70) Xu, H.; Sun, J.; Qin, A.; Hua, J.; Li, Z.; Dong, Y.; Xu, H.; Yuan, W.; Ma, Y.; Wang, M.; Tang, B. Z. Functional Perovskite Hybrid of Polyacetylene Ammonium and Lead Bromide: Synthesis, Light Emission, and Fluorescence Imagining. *J. Phys. Chem. B* **2006**, *110* (43), 21701–21709.
- (71) Chen, W.; Shi, Y.; Chen, J.; Ma, P.; Fang, Z.; Ye, D.; Lu, Y.; Yuan, Y.; Zhao, J.; Xiao, Z. Polymerized Hybrid Perovskites with Enhanced Stability, Flexibility, and Lattice Rigidity. *Adv. Mater.* **2021**, 33 (48), 2104842.
- (72) Ortiz-Cervantes, C.; Román-Román, P. I.; Vazquez-Chavez, J.; Hernández-Rodríguez, M.; Solis-Ibarra, D. Thousand-fold Conductivity Increase in 2D Perovskites by Polydiacetylene Incorporation and Doping. *Angew. Chem.*, Int. Ed. 2018, 130 (42), 14078–14082.
- (73) Kikuchi, K.; Takeoka, Y.; Rikukawa, M.; Sanui, K. Fabrication and Characterization of Organic-Inorganic Perovskite Films Containing Fullerene Derivatives. *Colloids Surf. A Physicochem. Eng. Asp.* **2005**, 257, 199–202.
- (74) Zhao, X.; Ball, M. L.; Kakekhani, A.; Liu, T.; Rappe, A. M.; Loo, Y. L. A Charge Transfer Framework That Describes Supramolecular Interactions Governing Structure and Properties of 2D Perovskites. *Nat. Commun.* **2022**, *13* (1), 3970.
- (75) Ren, H.; Yu, S.; Chao, L.; Xia, Y.; Sun, Y.; Zuo, S.; Li, F.; Niu, T.; Yang, Y.; Ju, H.; Li, B.; Du, H.; Gao, X.; Zhang, J.; Wang, J.; Zhang, L.; Chen, Y.; Huang, W. Efficient and Stable Ruddlesden-Popper Perovskite Solar Cell with Tailored Interlayer Molecular Interaction. *Nat. Photonics.* **2020**, *14* (3), 154–163.
- (76) Jana, M. K.; Liu, C.; Lidin, S.; Dirkes, D. J.; You, W.; Blum, V.; Mitzi, D. B. Resolving Rotational Stacking Disorder and Electronic Level Alignment in a 2D Oligothiophene-Based Lead Iodide Perovskite. *Chem. Mater.* **2019**, *31* (20), 8523–8532.
- (77) Saparov, B.; Mitzi, D. B. Organic-Inorganic Perovskites: Structural Versatility for Functional Materials Design. *Chem. Rev.* **2016**, *116* (7), 4558–4596.
- (78) Shi, E.; Yuan, B.; Shiring, S. B.; Gao, Y.; Akriti; Guo, Y.; Su, C.; Lai, M.; Yang, P.; Kong, J.; Savoie, B. M.; Yu, Y.; Dou, L. Two-Dimensional Halide Perovskite Lateral Epitaxial Heterostructures. *Nature* **2020**, *580* (7805), *614–620*.

- (79) Huang, Q.; Lin, Z.; Yan, D. Tuning Organic Room-Temperature Phosphorescence through the Confinement Effect of Inorganic Micro/Nanostructures. *Small Struct.* **2021**, *2* (9), 2100044.
- (80) Mitzi, D. B.; Wang, S.; Feild, C. A.; Chess, C. A.; Guloy, A. M. Conducting Layered Organic-Inorganic Halides Containing (110)-Oriented Perovskite Sheets. *Science* **1995**, 267 (5203), 1473–1476.
- (81) Mitzi, D. B. Synthesis, Crystal Structure, and Optical and Thermal Properties of $(C_4H_9NH_3)_2MI_4$ (M = Ge, Sn, Pb). *Chem. Mater.* **1996**, 8 (3), 791–800.
- (82) Tian, H.; Zhao, L.; Wang, X.; Yeh, Y. W.; Yao, N.; Rand, B. P.; Ren, T. L. Extremely Low Operating Current Resistive Memory Based on Exfoliated 2D Perovskite Single Crystals for Neuromorphic Computing. ACS Nano 2017, 11 (12), 12247–12256.
- (83) Zhang, Y.; Liu, Y.; Xu, Z.; Ye, H.; Li, Q.; Hu, M.; Yang, Z.; Liu, S. Two-Dimensional (PEA)₂ PbBr₄ Perovskite Single Crystals for a High Performance UV-Detector. *J. Mater. Chem. C* **2019**, 7 (6), 1584–1591.
- (84) Liu, Y.; Ye, H.; Zhang, Y.; Zhao, K.; Yang, Z.; Yuan, Y.; Wu, H.; Zhao, G.; Yang, Z.; Tang, J.; Xu, Z.; Liu, S. Surface-Tension-Controlled Crystallization for High-Quality 2D Perovskite Single Crystals for Ultrahigh Photodetection. *Matter* **2019**, *1* (2), 465–480.
- (85) Stoumpos, C. C.; Cao, D. H.; Clark, D. J.; Young, J.; Rondinelli, J. M.; Jang, J. I.; Hupp, J. T.; Kanatzidis, M. G. Ruddlesden-Popper Hybrid Lead Iodide Perovskite 2D Homologous Semiconductors. *Chem. Mater.* **2016**, 28 (8), 2852–2867.
- (86) Mao, L.; Kennard, R. M.; Traore, B.; Ke, W.; Katan, C.; Even, J.; Chabinyc, M. L.; Stoumpos, C. C.; Kanatzidis, M. G. Seven-Layered 2D Hybrid Lead Iodide Perovskites. *Chem.* **2019**, 5 (10), 2593–2604.
- (87) Park, J. Y.; Song, R.; Liang, J.; Jin, L.; Wang, K.; Li, S.; Shi, E.; Gao, Y.; Zeller, M.; Teat, J. S.; Guo, P.; Huang, L.; Zhao, Y. S.; Blum, V.; Dou, L. Dimensionality-Controlled Organic Semiconductor-Incorporated Perovskite Quantum Wells. *Nat. Chem.* **2023**, DOI: 10.1038/s41557-023-01311-0.
- (88) Samet, A.; Triki, S.; Abid, Y. Resonantly Enhanced White-Light Emission Involving Energy and Charge Transfer in One-Dimensional Hybrid Material: (ABT)₂[PbBr₃]. *J. Phys. Chem. C* **2019**, *123* (10), 6213–6219.
- (89) Long, Y.; Xian, Y.; Yuan, S.; Liu, K.; Sun, M.; Guo, Y.; Rahman, N. U.; Fan, J.; Li, W. π-π Conjugate Structure Enabling the Channel Construction of Carrier-Facilitated Transport in 1D-3D Multidimensional CsPbI₂Br Solar Cells with High Stability. *Nano Energy* **2021**, 89, 106340.
- (90) Wang, D.; Chen, J.; Zhu, P.; Qiao, Y.; Hu, H.; Zeng, J.; Zhang, J.; Qu, G.; Wang, Y.; Wang, X.; Jen, A. K. Y.; Xu, B. Binary Microcrystal Additives Enabled Antisolvent-Free Perovskite Solar Cells with High Efficiency and Stability. *Adv. Energy Mater.* **2023**, *13* (7), 2203649.
- (91) Fujisawa, J. I.; Giorgi, G. Lead-Iodide Nanowire Perovskite with Methylviologen Showing Interfacial Charge-Transfer Absorption: A DFT Analysis. *Phys. Chem. Chem. Phys.* **2014**, *16* (33), 17955–17959.
- (92) Tremblay, M. H.; Boyington, A.; Rigin, S.; Jiang, J.; Bacsa, J.; Al Kurdi, K.; Khrustalev, V. N.; Pachter, R.; Timofeeva, T. V.; Jui, N.; Barlow, S.; Marder, S. R. Hybrid Organic Lead Iodides: Role of Organic Cation Structure in Obtaining 1D Chains of Face-Sharing Octahedra vs 2D Perovskites. *Chem. Mater.* **2022**, *34* (3), 935–946.
- (93) Tremblay, M. H.; Zeidell, A. M.; Rigin, S.; Tyznik, C.; Bacsa, J.; Zhang, Y.; Al Kurdi, K.; Jurchescu, O. D.; Timofeeva, T. V.; Barlow, S.; Marder, S. R. Structural Diversity in 2,2'-[Naphthalene-1,8:4,5-Bis(Dicarboximide)- N,N'-Diyl]-Bis(Ethylammonium) Iodoplumbates. *Inorg. Chem.* **2020**, *59* (12), 8070–8080.
- (94) Amerling, E.; Zhai, Y.; Larson, B. W.; Yao, Y.; Fluegel, B.; Owczarczyk, Z.; Lu, H.; Whittaker-Brooks, L.; Blum, V.; Blackburn, J. L. Charge Transfer States and Carrier Generation in 1D Organolead Iodide Semiconductors. *J. Mater. Chem. A* **2021**, *9* (26), 14977–14990
- (95) Pious, J. K.; Basavarajappa, M. G.; Muthu, C.; Krishna, N.; Nishikubo, R.; Saeki, A.; Chakraborty, S.; Vijayakumar, C. Anisotropic Photoconductivity and Long-Lived Charge Carriers in Bismuth-Based

- One-Dimensional Perovskite with Type-IIa Band Alignment. J. Phys. Chem. Lett. 2020, 11 (16), 6757–6762.
- (96) Wudl, F.; Smith, G. M.; Hufnagel, E. J. Bis-1,3-Dithiolium Chloride: An Unusually Stable Organic Radical Cation. *J. Chem. Soc.* D 1970, 1453–1454.
- (97) Evans, H. A.; Lehner, A. J.; Labram, J. G.; Fabini, D. H.; Barreda, O.; Smock, S. R.; Wu, G.; Chabinyc, M. L.; Seshadri, R.; Wudl, F. (TTF)Pb₂I₅: A Radical Cation-Stabilized Hybrid Lead Iodide with Synergistic Optoelectronic Signatures. *Chem. Mater.* **2016**, 28 (11), 3607–3611.
- (98) Smith, M. D.; Jaffe, A.; Dohner, E. R.; Lindenberg, A. M.; Karunadasa, H. I. Structural Origins of Broadband Emission from Layered Pb-Br Hybrid Perovskites. *Chem. Sci.* **2017**, 8 (6), 4497–4504
- (99) Smith, M. D.; Karunadasa, H. I. White-Light Emission from Layered Halide Perovskites. *Acc. Chem. Res.* **2018**, *51* (3), *619*–*627*. (100) Yuan, Z.; Zhou, C.; Tian, Y.; Shu, Y.; Messier, J.; Wang, J. C.; Van De Burgt, L. J.; Kountouriotis, K.; Xin, Y.; Holt, E.; Schanze, K.; Clark, R.; Siegrist, T.; Ma, B. One-Dimensional Organic Lead Halide Perovskites with Efficient Bluish White-Light Emission. *Nat. Commun.* **2017**, *8* (1), 14051–14058.
- (101) Goldschmidt, V. M. Die Gesetze Der Krystallochemie. *Naturwissenschaften* **1926**, 14 (21), 477–485.
- (102) Lyu, R.; Moore, C. E.; Liu, T.; Yu, Y.; Wu, Y. Predictive Design Model for Low-Dimensional Organic-Inorganic Halide Perovskites Assisted by Machine Learning. J. Am. Chem. Soc. 2021, 143 (32), 12766–12776.
- (103) Mercier, N.; Poiroux, S.; Riou, A.; Batail, P. Unique Hydrogen Bonding Correlating with a Reduced Band Gap and Phase Transition in the Hybrid Perovskites $(HO(CH_2)_2NH_3)_2PbX_4$ (X = I, Br). *Inorg. Chem.* **2004**, 43 (26), 8361–8366.
- (104) Spanopoulos, I.; Hadar, I.; Ke, W.; Tu, Q.; Chen, M.; Tsai, H.; He, Y.; Shekhawat, G.; Dravid, V. P.; Wasielewski, M. R.; Mohite, A. D.; Stoumpos, C. C.; Kanatzidis, M. G. Uniaxial Expansion of the 2D Ruddlesden-Popper Perovskite Family for Improved Environmental Stability. *J. Am. Chem. Soc.* 2019, 141 (13), 5518–5534.
- (105) Hoffman, J. M.; Che, X.; Sidhik, S.; Li, X.; Hadar, I.; Blancon, J. C.; Yamaguchi, H.; Kepenekian, M.; Katan, C.; Even, J.; Stoumpos, C. C.; Mohite, A. D.; Kanatzidis, M. G. From 2D to 1D Electronic Dimensionality in Halide Perovskites with Stepped and Flat Layers Using Propylammonium as a Spacer. J. Am. Chem. Soc. 2019, 141 (27), 10661–10676.
- (106) Meuwly, M. Machine Learning for Chemical Reactions. *Chem. Rev.* **2021**, *121* (16), 10218–10239.
- (107) Pilania, G.; Mannodi-Kanakkithodi, A.; Uberuaga, B. P.; Ramprasad, R.; Gubernatis, J. E.; Lookman, T. Machine Learning Bandgaps of Double Perovskites. *Sci. Rep.* **2016**, *6* (1), 19375.
- (108) Artrith, N.; Butler, K. T.; Coudert, F. X.; Han, S.; Isayev, O.; Jain, A.; Walsh, A. Best Practices in Machine Learning for Chemistry. *Nat. Chem.* **2021**, *13* (6), 505–508.
- (109) Mater, A. C.; Coote, M. L. Deep Learning in Chemistry. *J. Chem. Inf. Model.* **2019**, 59 (6), 2545–2559.
- (110) Yu, Y.; Tan, X.; Ning, S.; Wu, Y. Machine Learning for Understanding Compatibility of Organic-Inorganic Hybrid Perovskites with Post-Treatment Amines. *ACS Energy Lett.* **2019**, *4* (2), 397–404.
- (111) Marchenko, E. I.; Fateev, S. A.; Petrov, A. A.; Korolev, V. V.; Mitrofanov, A.; Petrov, A. V.; Goodilin, E. A.; Tarasov, A. B. Database of Two-Dimensional Hybrid Perovskite Materials: Open-Access Collection of Crystal Structures, Band Gaps, and Atomic Partial Charges Predicted by Machine Learning. *Chem. Mater.* **2020**, 32 (17), 7383–7388.
- (112) Saidi, W. A.; Shadid, W.; Castelli, I. E. Machine-Learning Structural and Electronic Properties of Metal Halide Perovskites Using a Hierarchical Convolutional Neural Network. *NPJ. Comput. Mater.* **2020**, *6* (1), 36.
- (113) Li, Y.; Yang, J.; Zhao, R.; Zhang, Y.; Wang, X.; He, X.; Fu, Y.; Zhang, L. Design of Organic-Inorganic Hybrid Heterostructured Semiconductors via High-Throughput Materials Screening for

- Optoelectronic Applications. J. Am. Chem. Soc. 2022, 144 (36), 16656–16666.
- (114) Zhang, L.; Hu, W.; He, M.; Xu, K.; Pan, Z. Interpretable Machine Learning for Investigating Photoelectrochemical Properties of Cosensitizer-Based CH₃NH₃PbI₃/TiO₂ Films in Water. *J. Phys. Chem. C* **2022**, *126* (14), 6482–6490.
- (115) Lu, S.; Zhou, Q.; Ouyang, Y.; Guo, Y.; Li, Q.; Wang, J. Accelerated Discovery of Stable Lead-Free Hybrid Organic-Inorganic Perovskites via Machine Learning. *Nat. Commun.* **2018**, 9 (1), 3405.
- (116) Lin, Z.; Sun, J.; Shiring, S. B.; Dou, L.; Savoie, B. M. Design Rules for Two-Dimensional Organic Semiconductor-Incorporated Perovskites (OSiP) Gleaned from Thousands of Simulated Structures. *Angew. Chem., Int. Ed* 2023, 62, e202305298.
- (117) Deng, S.; Shi, E.; Yuan, L.; Jin, L.; Dou, L.; Huang, L. Long-Range Exciton Transport and Slow Annihilation in Two-Dimensional Hybrid Perovskites. *Nat. Commun.* **2020**, *11* (1), 664.
- (118) Cao, F.; Yu, D.; Telychko, M.; Lu, J.; Pang, P.; Su, C.; Xing, G. Navigating the Site-Distinct Energy Conversion Properties of Perovskite Quantum Wells. ACS Energy Lett. 2023, 8 (2), 1236–1265.
- (119) Hong, X.; Ishihara, T.; Nurmikko, A. V. Dielectric Confinement Effect on Excitons in PbI₄-Based Layered Semiconductors. *Phys. Rev. B* **1992**, *45* (12), 6961.
- (120) Tanaka, K.; Sano, F.; Takahashi, T.; Kondo, T.; Ito, R.; Ema, K. Two-Dimensional Wannier Excitons in a Layered-Perovskite-Type Crystal $(C_6H_{13}NH_3)_2PbI_4$. Solid State Commun. **2002**, 122 (5), 249–252
- (121) Blancon, J. C.; Stier, A. V.; Tsai, H.; Nie, W.; Stoumpos, C. C.; Traoré, B.; Pedesseau, L.; Kepenekian, M.; Katsutani, F.; Noe, G. T.; Kono, J.; Tretiak, S.; Crooker, S. A.; Katan, C.; Kanatzidis, M. G.; Crochet, J. J.; Even, J.; Mohite, A. D. Scaling Law for Excitons in 2D Perovskite Quantum Wells. *Nat. Commun.* **2018**, 9 (1), 2254.
- (122) Goyal, A.; McKechnie, S.; Pashov, D.; Tumas, W.; Van Schilfgaarde, M.; Stevanović, V. Origin of Pronounced Nonlinear Band Gap Behavior in Lead-Tin Hybrid Perovskite Alloys. *Chem. Mater.* **2018**, *30* (11), 3920–3928.
- (123) Deng, S.; Snaider, J. M.; Gao, Y.; Shi, E.; Jin, L.; Schaller, R. D.; Dou, L.; Huang, L. Long-Lived Charge Separation in Two-Dimensional Ligand-Perovskite Heterostructures. *J. Chem. Phys.* **2020**, 152 (4), 044711.
- (124) Yang, Y.; Liu, C.; Syzgantseva, O. A.; Syzgantseva, M. A.; Ma, S.; Ding, Y.; Cai, M.; Liu, X.; Dai, S.; Nazeeruddin, M. K. Defect Suppression in Oriented 2D Perovskite Solar Cells with Efficiency over 18% via Rerouting Crystallization Pathway. *Adv. Energy Mater.* **2021**, *11* (1), 2002966.
- (125) Zhang, X.; Wu, G.; Fu, W.; Qin, M.; Yang, W.; Yan, J.; Zhang, Z.; Lu, X.; Chen, H. Orientation Regulation of Phenylethylammonium Cation Based 2D Perovskite Solar Cell with Efficiency Higher Than 11%. *Adv. Energy Mater.* **2018**, *8* (14), 1702498.
- (126) Zhang, F.; Park, S. Y.; Yao, C.; Lu, H.; Dunfield, S. P.; Xiao, C.; Uličná, S.; Zhao, X.; Du Hill, L.; Chen, X.; Wang, X.; Mundt, L. E.; Stone, K. H.; Schelhas, L. T.; Teeter, G.; Parkin, S.; Ratcliff, E. L.; Loo, Y. L.; Berry, J. J.; Beard, M. C.; Yan, Y.; Larson, B. W.; Zhu, K. Metastable Dion-Jacobson 2D Structure Enables Efficient and Stable Perovskite Solar Cells. *Science* 2022, 375 (6576), 71–76.
- (127) Zhang, F.; Kim, D. H.; Lu, H.; Park, J. S.; Larson, B. W.; Hu, J.; Gao, L.; Xiao, C.; Reid, O. G.; Chen, X.; Zhao, Q.; Ndione, P. F.; Berry, J. J.; You, W.; Walsh, A.; Beard, M. C.; Zhu, K. Enhanced Charge Transport in 2D Perovskites via Fluorination of Organic Cation. J. Am. Chem. Soc. 2019, 141 (14), 5972–5979.
- (128) Jiang, Q.; Tong, J.; Xian, Y.; Kerner, R. A.; Dunfield, S. P.; Xiao, C.; Scheidt, R. A.; Kuciauskas, D.; Wang, X.; Hautzinger, M. P.; Tirawat, R.; Beard, M. C.; Fenning, D. P.; Berry, J. J.; Larson, B. W.; Yan, Y.; Zhu, K. Surface Reaction for Efficient and Stable Inverted Perovskite Solar Cells. *Nature* **2022**, *611* (7935), 278–283.
- (129) Gélvez-Rueda, M. C.; Fridriksson, M. B.; Dubey, R. K.; Jager, W. F.; van der Stam, W.; Grozema, F. C. Overcoming the Exciton Binding Energy in Two-Dimensional Perovskite Nanoplatelets by Attachment of Conjugated Organic Chromophores. *Nat. Commun.* **2020**, *11* (1), 1901.

- (130) Wang, K.; Wu, C.; Jiang, Y.; Yang, D.; Wang, K.; Priya, S. Distinct Conducting Layer Edge States in Two-Dimensional (2D) Halide Perovskite. *Sci. Adv.* **2019**, *5* (7), No. eaau3241.
- (131) Dong, H.; Ran, C.; Gao, W.; Sun, N.; Liu, X.; Xia, Y.; Chen, Y.; Huang, W. Crystallization Dynamics of Sn-Based Perovskite Thin Films: Toward Efficient and Stable Photovoltaic Devices. *Adv. Energy Mater.* **2022**, *12* (1), 2102213.
- (132) Akriti; Shi, E.; Shiring, S. B.; Yang, J.; Atencio-Martinez, C. L.; Yuan, B.; Hu, X.; Gao, Y.; Finkenauer, B. P.; Pistone, A. J.; Yu, Y.; Liao, P.; Savoie, B. M.; Dou, L. Layer-by-Layer Anionic Diffusion in Two-Dimensional Halide Perovskite Vertical Heterostructures. *Nat. Nanotechnol.* **2021**, *16* (5), 584–591.
- (133) Akriti; Zhang, S.; Lin, Z. Y.; Shi, E.; Finkenauer, B. P.; Gao, Y.; Pistone, A. J.; Ma, K.; Savoie, B. M.; Dou, L. Quantifying Anionic Diffusion in 2D Halide Perovskite Lateral Heterostructures. *Adv. Mater.* **2021**, 33 (51), 2105183.
- (134) Hu, J.; Oswald, I. W. H.; Stuard, S. J.; Nahid, M. M.; Zhou, N.; Williams, O. F.; Guo, Z.; Yan, L.; Hu, H.; Chen, Z.; Xiao, X.; Lin, Y.; Yang, Z.; Huang, J.; Moran, A. M.; Ade, H.; Neilson, J. R.; You, W. Synthetic Control over Orientational Degeneracy of Spacer Cations Enhances Solar Cell Efficiency in Two-Dimensional Perovskites. *Nat. Commun.* **2019**, *10* (1), 1276.
- (135) Ni, C.; Huang, Y.; Zeng, T.; Chen, D.; Chen, H.; Wei, M.; Johnston, A.; Proppe, A. H.; Ning, Z.; Sargent, E. H.; Hu, P.; Yang, Z. Thiophene Cation Intercalation to Improve Band-Edge Integrity in Reduced-Dimensional Perovskites. *Angew. Chem., Int. Ed.* **2020**, *132* (33), 14081–14087.
- (136) Chen, H.; Teale, S.; Chen, B.; Hou, Y.; Grater, L.; Zhu, T.; Bertens, K.; Park, S. M.; Atapattu, H. R.; Gao, Y.; Wei, M.; Johnston, A. K.; Zhou, Q.; Xu, K.; Yu, D.; Han, C.; Cui, T.; Jung, E. H.; Zhou, C.; Zhou, W.; Proppe, A. H.; Hoogland, S.; Laquai, F.; Filleter, T.; Graham, K. R.; Ning, Z.; Sargent, E. H. Quantum-Size-Tuned Heterostructures Enable Efficient and Stable Inverted Perovskite Solar Cells. *Nat. Photonics* **2022**, *16* (5), 352–358.
- (137) Jang, Y. W.; Lee, S.; Yeom, K. M.; Jeong, K.; Choi, K.; Choi, M.; Noh, J. H. Intact 2D/3D Halide Junction Perovskite Solar Cells via Solid-Phase in-Plane Growth. *Nat. Energy* **2021**, *6* (1), 63–71.
- (138) Dong, H.; Xi, J.; Zuo, L.; Li, J.; Yang, Y.; Wang, D.; Yu, Y.; Ma, L.; Ran, C.; Gao, W.; Jiao, B.; Xu, J.; Lei, T.; Wei, F.; Yuan, F.; Zhang, L.; Shi, Y.; Hou, X.; Wu, Z. Conjugated Molecules "Bridge": Functional Ligand toward Highly Efficient and Long-Term Stable Perovskite Solar Cell. Adv. Funct. Mater. 2019, 29 (17), 1808119.
- (139) Liu, G.; Zheng, H.; Ye, J.; Xu, S.; Zhang, L.; Xu, H.; Liang, Z.; Chen, X.; Pan, X. Mixed-Phase Low-Dimensional Perovskite-Assisted Interfacial Lead Directional Management for Stable Perovskite Solar Cells with Efficiency over 24%. ACS Energy Lett. 2021, 6 (12), 4395–4404.
- (140) Wang, N.; Cheng, L.; Ge, R.; Zhang, S.; Miao, Y.; Zou, W.; Yi, C.; Sun, Y.; Cao, Y.; Yang, R.; Wei, Y.; Guo, Q.; Ke, Y.; Yu, M.; Jin, Y.; Liu, Y.; Ding, Q.; Di, D.; Yang, L.; Xing, G.; Tian, H.; Jin, C.; Gao, F.; Friend, R. H.; Wang, J.; Huang, W. Perovskite Light-Emitting Diodes Based on Solution-Processed Self-Organized Multiple Quantum Wells. *Nat. Photonics* **2016**, *10* (11), 699–704.
- (141) Yuan, M.; Quan, L. N.; Comin, R.; Walters, G.; Sabatini, R.; Voznyy, O.; Hoogland, S.; Zhao, Y.; Beauregard, E. M.; Kanjanaboos, P.; Lu, Z.; Kim, D. H.; Sargent, E. H. Perovskite Energy Funnels for Efficient Light-Emitting Diodes. *Nat. Nanotechnol.* **2016**, *11* (10), 872–877.
- (142) Byun, J.; Cho, H.; Wolf, C.; Jang, M.; Sadhanala, A.; Friend, R. H.; Yang, H.; Lee, T. W. Efficient Visible Quasi-2D Perovskite Light-Emitting Diodes. *Adv. Mater.* **2016**, 28 (34), 7515–7520.
- (143) Kong, L.; Zhang, X.; Li, Y.; Wang, H.; Jiang, Y.; Wang, S.; You, M.; Zhang, C.; Zhang, T.; Kershaw, S. V.; Zheng, W.; Yang, Y.; Lin, Q.; Yuan, M.; Rogach, A. L.; Yang, X. Smoothing the Energy Transfer Pathway in Quasi-2D Perovskite Films Using Methanesulfonate Leads to Highly Efficient Light-Emitting Devices. *Nat. Commun.* 2021, 12 (1), 1246.
- (144) Chen, H.; Lin, J.; Kang, J.; Kong, Q.; Lu, D.; Kang, J.; Lai, M.; Quan, L. N.; Lin, Z.; Jin, J.; Wang, L. W.; Toney, M. F.; Yang, P.

- Structural and Spectral Dynamics of Single-Crystalline Ruddlesden-Popper Phase Halide Perovskite Blue Light-Emitting Diodes. *Sci. Adv.* **2020**, *6* (4), No. eaay4045.
- (145) Qin, C.; Matsushima, T.; Potscavage, W. J.; Sandanayaka, A. S. D.; Leyden, M. R.; Bencheikh, F.; Goushi, K.; Mathevet, F.; Heinrich, B.; Yumoto, G.; Kanemitsu, Y.; Adachi, C. Triplet Management for Efficient Perovskite Light-Emitting Diodes. *Nat. Photonics* **2020**, *14* (2), 70–75.
- (146) Yang, X.; Zhang, X.; Deng, J.; Chu, Z.; Jiang, Q.; Meng, J.; Wang, P.; Zhang, L.; Yin, Z.; You, J. Efficient Green Light-Emitting Diodes Based on Quasi-Two-Dimensional Composition and Phase Engineered Perovskite with Surface Passivation. *Nat. Commun.* **2018**, 9 (1), 570.
- (147) Guo, Y.; Apergi, S.; Li, N.; Chen, M.; Yin, C.; Yuan, Z.; Gao, F.; Xie, F.; Brocks, G.; Tao, S.; Zhao, N. Phenylalkylammonium Passivation Enables Perovskite Light Emitting Diodes with Record High-Radiance Operational Lifetime: The Chain Length Matters. *Nat. Commun.* 2021, 12 (1), 644.
- (148) Ban, M.; Zou, Y.; Rivett, J. P. H.; Yang, Y.; Thomas, T. H.; Tan, Y.; Song, T.; Gao, X.; Credgington, D.; Deschler, F.; Sirringhaus, H.; Sun, B. Solution-Processed Perovskite Light Emitting Diodes with Efficiency Exceeding 15% through Additive-Controlled Nanostructure Tailoring. *Nat. Commun.* **2018**, *9* (1), 3892.
- (149) Quan, L. N.; Ma, D.; Zhao, Y.; Voznyy, O.; Yuan, H.; Bladt, E.; Pan, J.; García de Arquer, F. P.; Sabatini, R.; Piontkowski, Z.; Emwas, A. H.; Todorović, P.; Quintero-Bermudez, R.; Walters, G.; Fan, J. Z.; Liu, M.; Tan, H.; Saidaminov, M. I.; Gao, L.; Li, Y.; Anjum, D. H.; Wei, N.; Tang, J.; McCamant, D. W.; Roeffaers, M. B. J.; Bals, S.; Hofkens, J.; Bakr, O. M.; Lu, Z. H.; Sargent, E. H. Edge Stabilization in Reduced-Dimensional Perovskites. *Nat. Commun.* 2020, 11 (1), 170.
- (150) Matsushima, T.; Leyden, M. R.; Fujihara, T.; Qin, C.; Sandanayaka, A. S. D.; Adachi, C. Large Metal Halide Perovskite Crystals for Field-Effect Transistor Applications. *Appl. Phys. Lett.* **2019**, *115* (12), 120601.
- (151) Zhu, H.; Liu, A.; Shim, K. I.; Hong, J.; Han, J. W.; Noh, Y. Y. High-Performance and Reliable Lead-Free Layered-Perovskite Transistors. *Adv. Mater.* **2020**, 32 (31), 2002717.
- (152) Matsushima, T.; Hwang, S.; Sandanayaka, A. S. D.; Qin, C.; Terakawa, S.; Fujihara, T.; Yahiro, M.; Adachi, C. Solution-Processed Organic-Inorganic Perovskite Field-Effect Transistors with High Hole Mobilities. *Adv. Mater.* **2016**, 28 (46), 10275–10281.
- (153) Mitzi, D. B.; Dimitrakopoulos, C. D.; Rosner, J.; Medeiros, D. R.; Xu, Z.; Noyan, C. Hybrid Field-Effect Transistor Based on a Low-Temperature Melt-Processed Channel Layer. *Adv. Mater.* **2002**, *14* (23), 1772–1776.
- (154) Zhao, L.; Lin, Y. L.; Kim, H.; Giebink, N. C.; Rand, B. P. Donor/Acceptor Charge-Transfer States at Two-Dimensional Metal Halide Perovskite and Organic Semiconductor Interfaces. *ACS Energy Lett.* **2018**, 3 (11), 2708–2712.
- (155) Yurash, B.; Cao, D. X.; Brus, V. V.; Leifert, D.; Wang, M.; Dixon, A.; Seifrid, M.; Mansour, A. E.; Lungwitz, D.; Liu, T.; Santiago, P. J.; Graham, K. R.; Koch, N.; Bazan, G. C.; Nguyen, T. Q. Towards Understanding the Doping Mechanism of Organic Semiconductors by Lewis Acids. *Nat. Mater.* **2019**, *18* (12), 1327–1334.
- (156) Tietze, M. L.; Benduhn, J.; Pahner, P.; Nell, B.; Schwarze, M.; Kleemann, H.; Krammer, M.; Zojer, K.; Vandewal, K.; Leo, K. Elementary Steps in Electrical Doping of Organic Semiconductors. *Nat. Commun.* **2018**, *9* (1), 1182.
- (157) Lin, X.; Wegner, B.; Lee, K. M.; Fusella, M. A.; Zhang, F.; Moudgil, K.; Rand, B. P.; Barlow, S.; Marder, S. R.; Koch, N.; Kahn, A. Beating the Thermodynamic Limit with Photo-Activation of n-Doping in Organic Semiconductors. *Nat. Mater.* **2017**, *16* (12), 1209–1215.
- (158) Liu, G.; Gong, J.; Kong, L.; Schaller, R. D.; Hu, Q.; Liu, Z.; Yan, S.; Yang, W.; Stoumpos, C. C.; Kanatzidis, M. G.; Mao, H. K.; Xu, T. Isothermal Pressure-Derived Metastable States in 2D Hybrid Perovskites Showing Enduring Bandgap Narrowing. *Proc. Natl. Acad. Sci. U.S.A.* 2018, 115 (32), 8076–8081.

- (159) Muscarella, L. A.; Dučinskas, A.; Dankl, M.; Andrzejewski, M.; Casati, N. P. M.; Rothlisberger, U.; Maier, J.; Graetzel, M.; Ehrler, B.; Milić, J. V. Reversible Pressure-Dependent Mechanochromism of Dion-Jacobson and Ruddlesden-Popper Layered Hybrid Perovskites. *Adv. Mater.* **2022**, *34* (17), 2108720.
- (160) Guo, S.; Li, Y.; Mao, Y.; Tao, W.; Bu, K.; Fu, T.; Zhao, C.; Luo, H.; Hu, Q.; Zhu, H.; Shi, E.; Yang, W.; Dou, L.; Lü, X. Reconfiguring Band-Edge States and Charge Distribution of Organic Semiconductor-Incorporated 2D Perovskites via Pressure Gating. *Sci. Adv.* 2022, 8 (44), No. eadd1984.
- (161) Lemmerer, A.; Billing, D. G. Synthesis, Characterization and Phase Transitions of the Inorganic-Organic Layered Perovskite-Type Hybrids $[(C_nH_{2n+1}NH_3)_2PbI_4]$, n = 7, 8, 9 and 10. *Dalton Trans.* **2012**, *41* (4), 1146–1157.